Informational Entropy and the Stability of Barotropic Atmospheric Flow

Valentin P. Dymnikov[1], Viacheslav V. Kharin[2]

and Hans von Storch[2]

1. Institute of Numerical Mathematics of the Russian Academy of Sciences

Leninsky Prospect 32A, 117334 Moscow, Russia

2. Max-Planck-Institut für Meteorologie

Bundesstrasse 55, 20146 Hamburg, Germany

Abstract

Two informational entropy measures which exploit the geometry of the instantaneous 500 *mb* vorticiy field either in geometrical ($E(\rho_1)$) or energetic coordinates ($E(\rho_2)$) are introduced. They are compared with a series of conceptually different parameters characterizing extratropical atmospheric flow fields which can be considered as stability measures for atmospheric states under certain conditions:

- the enstrophy η and the mean squared wave number k^2,
- the sum L of positive instantaneous local Lyapunov exponents,
- the sum K of the positive eigenvalues of the operator in the equation for barotropic kinetic energy of disturbances, and
- the instability index I_3 introduced by Dymnikov et al. (1990).

Theoretical simplifying arguments indicate that for quasibarotropic flows the measures $E(\rho_1)$, η, L and K, defined on the hemisphere, as well as $E(\rho_2)$, k^2 and I_3, defined for any regions on the hemisphere, are related to each other.

We verified these hypotheses by examining a 30-year data set of daily 500 *mb* height fields of the entire extratropical Northern Hemisphere and of the North Atlantic/Western Europe sector. The Lyapunov-type measures L and K were calculated from 10-day mean states. The theoretical results were found to fit very good for the set $E(\rho_1)$, η, L, K, calculated for the Northern Hemisphere. The similarity of measures $E(\rho_2)$, k^2 and I_3 in the North Atlantic/Western Europe sector was found to be fair. Although the concept of informational entropy does not allow to classify uniquely atmospheric states in the synoptical sense ("grosswetterlagen"), the systematical differences between atmospheric flows with high, normal and low entropies are found.

1 Introduction

The concept of atmospheric circulation regimes allows the introduction of a regime distribution function by means of which we can define different climatic functionals. These functionals can then be used in estimating regional and global climate changes which is one of the important aspects of climatological studies. Therefore the introduction of the distribution function of atmospheric regimes for given regions seems to be an approach with a promising outlook.

The central problem in this direction is the definition of atmospheric circulation regimes. Dzerdzeevsky (1956) introduced, for example, about two dozen regimes. Blinova (1943) and Kats (1960) constructed circulation indices which characterize meridional and zonal types of circulation. In the last twenty years much attention has been paid to studies of "blocking-type" regimes, which are quasistationary regional atmospheric circulation regimes with quasibarotropic structure. Many classifications of atmospheric circulation regimes have been done by means of cluster analysis methods (a technique which suffers from its dependence on the particular measure used). For limited areas, like the North Atlantic/Western Europe region, the approach successfully allows for the discrimination of regimes such as blocking and zonal flow (Legras et al., 1989). For the whole hemisphere the number of regimes is much larger and it is difficult to define their relationship to the blocking process (Molteni et al., 1990).

Comparing results of a cluster analysis with the stationary solutions of a barotropic model, Mo and Ghil (1987) showed that the centers of clusters were close to stationary points and that the lifetime of the trajectories in a cluster strongly depended on the distance from the center of the cluster. Since all the trajectories appeared to be unstable in the Lyapunov sense, such dependence is theoretically possible if the disturbance energy is equally probable distributed in orthogonal basis of unstable manifold of a stationary solution. This problem was discussed also in Dymnikov et al. (1990), Dymnikov (1990) and Dymnikov and Filatov (1990) where, on the base of observational data, an attempt was made to determine the relationship between the lifetime of quasistationary atmospheric circulation regimes like blockings and their stability characteristics.

In the present paper we approach the classification problem by studying the "informational entropy" (for the sake of brevity we will omit the word "informational" in the following) of

the atmospheric circulation for a geographically limited region and for the whole Northern Hemisphere. The concept of entropy as a description of atmospheric states is not new. Obukhov (1964) introduced a density distribution function characterizing the distribution of atmospheric mass with respect to the volumes formed by surfaces of constant potential vorticity and constant potential temperature. This distribution function was used by Kurgansky and Tatarskaya (1987) for a study of the annual cycle of the entropy for the FGGE data set.

Our purpose is not only to compute the entropy of atmospheric states and compare quasibarotropic atmospheric regimes using this notion but also to understand the relation of the entropy to stability characteristics of barotropic circulation, in particular, to local Lyapunov exponents (Dymnikov and Skiba, 1987; Frederiksen and Bell, 1990; Abarbanel et al. 1991). The first steps in this direction were undertaken by Dymnikov et al. (1992). The idea of classifying atmospheric regimes in terms of their informational entropy seems to be more productive in the analysis of regional types of atmospheric circulation, for instance, in the North Atlantic/Western Europe region. However in this case the analysis of the stability properties of regional circulation regimes seems to be more problematic than of the global circulation (Dymnikov et al., 1990).

The paper is organized as follows. In Section 2 different definitions of entropy are discussed and the notion of "E-regimes" is introduced. Time series of entropy for the North Atlantic/Western Europe region and for the Northern Hemisphere are calculated and discussed. Correlation relationships between the entropy, the enstrophy and the squared mean wave number of atmospheric states are also demonstrated. In Section 3 local Lyapunov exponents (for a barotropic atmosphere) and the instability index I_3, proposed by Dymnikov et al. (1990), are defined. Instantaneous local Lyapunov exponents, the instability index and the entropies are compared in Section 4. Conclusions and discussions of results follow in the last Section 5. Technical aspects of our work are gathered in a series of appendices.

2 Informational Entropy

We adopt the notion that the large-scale quasibarotropic dynamics of the extratropical troposphere may be represented by just one variable, namely the relative vorticity ξ. Consistent with this notion we will use throughout this paper the conventional barotropic vorticity equation as

dynamical framework:

$$\frac{\partial \xi}{\partial t} + J(\psi, \xi + f) + \alpha\xi + \mu\nabla^4\xi = F \tag{1}$$

where $\xi = \nabla^2\psi$ is the relative vorticity, ψ is the streamfunction and $f = 2\Omega sin\phi$ is the Coriolis parameter. α and μ are the linear drag and the horizontal diffusion coefficients, respectively. F stands for external forcing.

We use three integral quantities to characterize the state of the barotropic flow given by $\xi(t) = \nabla^2\psi$ at time t in the area D (with surface $|D|$): The enstrophy η, the total kinetic energy $|K|$ and the "mean squared wavenumber" k^2:

$$\eta(\xi(t)) = \frac{1}{|D|}\int_D \xi^2 dx \tag{2}$$

$$|K|(\xi(t)) = \frac{1}{|D|}\int_D |\nabla\psi|^2 dx \tag{3}$$

$$k^2(\xi(t)) = \frac{\eta}{|K|}. \tag{4}$$

The dimension of the phase space represented by ξ is infinite since the partial differential equations (1) can be transformed into an infinite system of ordinary differential equations, for example, by expanding ξ into a Fourier series in terms of spherical harmonics. In reality, however, we deal usually with a phase space of finite dimension. This could be either the phase space of a numerical solution of (1) or the phase space of data observed at discrete times and locations. In particular, the coordinates of the phase space can be chosen in a natural way as values of the relative vorticity at each grid point of the two-dimensional array of observed data.

For the computations throughout this paper we assume that 500 mb geopotential height represents sufficiently well the barotropic component, with the dynamics represented by (1). Height data is available on a $5^o \times 5^o$ latitude $\times$ longitude grid (provided by NCAR).

The conventional definition of the entropy of the atmospheric circulation operates with probability distribution values for each phase space coordinate (or at each grid point). For that purpose the whole time evolution of the solution at each grid point is considered. We take a different approach here by defining informational entropies as a characteristic parameter of individual points in the phase space, i.e., individual atmospheric states represented by one relative vorticity field $\xi(t)$ at some time t. One way to do that is to assume that at each time all phase coordinates (or grid points) are statistically equivalent and independent of each other. In this

case each concrete atmospheric state can be considered as an ensemble of independent realisations of relative vorticity in one-dimensional phase space. With the density of this ensemble labelled $\rho^{\xi}(r)$ we define the entropy of the field ξ as

$$E(\rho^{\xi}) = -\int_{-\infty}^{\infty} \rho^{\xi}(r) ln(\rho^{\xi}(r)) dr \tag{5}$$

The function ρ^{ξ} is named an *entropy density function.* A natural definition of E-regimes of atmospheric states is then accomplished by introducing the *regime density function* ρ_E through

$$\frac{1}{|T|} \int_{g^{-1}(\Omega_E)} dt = \int_{\Omega_E} \rho_E(E) dE \tag{6}$$

Ω_E is any set of entropies, $g(t)$ is the entropy at time t so that $g^{-1}(\Omega_E)$ is the time during which the system's entropy E is in Ω_E. The division by the total time $|T|$ is introduced to ensure that the integral of the density over the whole real line of possible entropies is one. If $\Omega_E = [E, E + \Delta E]$ is sufficiently small then $\rho_E(E) \approx \frac{1}{|T|} \frac{\sum \Delta t_k}{\Delta E}$ with Δt_k being the length of time intervals during which the entropy is in $[E, E + \Delta E]$.

The E-regime density function can be used as climatological functionals, for instance, for testing the ability of atmospheric general circulation models to reproduce the regional climate.

In the following we will introduce two definitions for the entropy density functions ρ^{ξ} of a given atmospheric state ξ. Both definitions apply, in principle, for any subarea of the extratropics. The entropy density function ρ_1 is formulated in terms of portions of area (Subsection 2.1), and ρ_2 in terms of portions of kinetic energy (Subsection 2.2).

2.1 The Definition of ρ_1

The density function ${\rho_1}^{\xi}$ of one gridded ξ-field is the relative number of realizations, or in our case, just the relative number of grid points with relative vorticity in the interval $(r, r + dr)$. Taking into account the area of grid boxes associated with each grid point the mathematical expression for the density $\rho_1 = {\rho_1}^{\xi(t)}(r)$ is given by

$$\frac{1}{|D|} \int_{\Omega_D} dx = \int_{v(\Omega_D)} {\rho_1}^{\xi}(r) dr \tag{7}$$

Here D is the full domain with the surface $|D|$, Ω_D is any subarea of D, $v(x)$ is the vorticity at the location x so that the set $v(\Omega_D)$ encompasses all vorticities at locations within Ω_D. The normalization with $\frac{1}{|D|}$ has been introduced to ensure $\int_{-\infty}^{\infty} \rho(r) dr = 1$.

If ${\rho_1}^\xi$ is Gaussian then its entropy $E(\rho_1)$ is proportional to the logarithm of the *enstrophy* η. For any two vorticity fields ξ and $c\xi$ with the same structure but different "amplitude" (represented by c) we find $E({\rho_1}^{c\xi}) > E({\rho_1}^\xi)$ if $c > 1$ and $E({\rho_1}^{c\xi}) < E({\rho_1}^\xi)$ if $c < 1$. In that sense the entropy $E(\rho_1)$ depends on the amplitude of the vorticity field. For the details, see Appendix A.

The mathematical object we have defined here has the *form* of an entropy, and we have therefore added the adjective "informational". We cannot automatically use properties of the well-founded thermodynamic concept of entropy. In the light of this limitation our somewhat dubious assumption about the equivalence of all grid boxes independent of their geographical locations appears less grave. This assumption would imply that only the regions with homogeneous conditions where all points are indistinguishable in the sense of their statistical properties have to be considered. On the other hand, the number of grid points, and consequently, the region should not be too small to compute the distribution function with a sufficient accuracy.

2.2 The Definition of ρ_2

The $E({\rho_1}^{\xi(t)})$-definition of the informational entropy of the state $\xi(t)$ given in the previous subsection is not fully satisfactory because of its sensitivity to disturbances with high vorticity but low energy, such as small scale analysis errors. This problem can be avoided by using a share of the kinetic energy instead of the area in the definition of the entropy density function and normalizing the relative vorticity field by the square root of the total kinetic energy of the atmospheric state, shifting in such a way all states to a single energy level. In this case we have a new definition of an entropy density function

$$\frac{1}{|K|}\int_{\Omega_K} dK = \int_{n(\Omega_K)} {\rho_2}^\xi(r^*)dr^* \tag{8}$$

Here $|K|$ is the total kinetic energy of the state $\xi(t)$, $K(x)$ is the kinetic energy at the location x. Ω_K is any set of kinetic energy values of the state ξ, and $n(\Omega_K)$ is the set of normalized relative vorticities $r^* = r/\sqrt{|K|}$ found at all locations x with $K(x) \in \Omega_K$.

If the entropy density function ${\rho_2}^\xi$ is Gaussian then $E(\rho_2)$ is a linear function of the logarithm of the mean squared wave number $k^2(\xi)$. The entropy $E(\rho_2)$ is independent of the amplitude of the pattern, i.e., $E({\rho_2}^{c\xi}) = E({\rho_2}^\xi)$. (For the details see Appendix B.)

2.3 Informational Entropy of Observed Circulation

In the following section we will present entropies computed for the 30-year interval from 1958 through 1987 for two areas. The first area, named "North Atlantic/Western Europe" and abbreviated "NAWE", covers $65^oW - 25^oE \times 30^oN - 80^oN$. We have chosen this region because it is often influenced by North Atlantic blockings. The second area is the Northern Hemisphere, abbreviated by "NH", poleward of 20^oN. We have calculated entropies for daily data and for 10-day mean data (to exclude the high frequency variability associated with baroclinic activity).

In the subsections 2.3.1 and 2.3.2 we deal with the two regions NAWE and NH, and in Subsection 2.3.3 we discuss the interannual variability of the entropies.

2.3.1 Results for the North Atlantic/Western Europe Region

Figure 1 shows the time behavior of entropies $E(\rho_1)$ and $E(\rho_2)$ computed for 10-day means and for daily data in the year 1985 together with their annual cycles computed as the first two Fourier harmonics. The entropies computed for daily data are larger than those computed for 10-day means. The richer spatial structure of instantaneous maps, compared to time-averaged maps, is revealed as an enhanced entropy. The two 10-day mean curves share the same variability on time scales of 30 to 90 days. The major local extremes are also present in the daily values. But the two measures $E(\rho_1)$ and $E(\rho_2)$ are different with respect to details and with respect to the annual cycle. The mean annual correlations of $E(\rho_1)$ and $E(\rho_2)$ are 0.53 on a daily basis and 0.60 on a 10-day basis (after subtraction of the annual cycles).

$E(\rho_1)$ has a summer minimum whereas the minimum of $E(\rho_2)$ is attained in winter. This at first glance puzzling behaviour reflects the different sensitivity of the two entropy definitions to "amplitude" variations. In winter the "amplitude" in the time mean vorticity field is larger than in summer. Therefore $E({\rho_1}^{\text{winter}}) > E({\rho_1}^{\text{summer}})$. $E(\rho_2)$, on the other hand, was found to be insensitive to changes of the "amplitude" and to represent the mean squared wave number, i.e., the inverse of a typical length scale. Therefore $E({\rho_2}^{\text{winter}}) \sim k^2(\text{winter}) < k^2(\text{summer}) \sim E({\rho_1}^{\text{summer}})$.

Figure 2 shows a scatter diagram of the entropies $E(\rho_1)$ and $E(\rho_2)$ calculated for all 10-day mean NAWE 500 *mb* height fields in winter (DJF). This scatter diagram indicates that for large,

or small, entropies the two measures yield similar results. There is no case of simultaneous, say, very large $E(\rho_1)$-entropy and very small $E(\rho_2)$-entropy.

From the scatter diagram in Figure 2 we have selected six 10-day mean 500 *mb* height fields as examples, three of them having large entropies and three having small entropies (Figure 3). In both definitions of the entropy density, $\rho = \rho_1$ and $\rho = \rho_2$, a circulation which deviates only weakly from a purely zonal flow has little entropy (Figure 3a-c), whereas isolated features, such as a cut-off low (Figure 3d), an elongated trough (Figure 3e) or a blocking (Figure 3f), go with high entropy. Similar results are obtained for summer (not shown).

We calculated the correlations $\langle ln(\eta), E(\rho_1)\rangle$ and $\langle ln(k^2), E(\rho_2)\rangle$ for each year for daily data and for 10-day means after having taken out the annual cycle by removing the first two annual harmonics. The multi-year averages of these correlations are:

	$\langle ln(\eta), E(\rho_1)\rangle$	$\langle ln(k^2), E(\rho_2)\rangle$
daily	0.85	0.82
10-day means	0.95	0.82

These high correlations empirically verify our theoretically based hypotheses that the entropy $E(\rho_1)$ and the logarithm of the enstrophy η as well as the entropy $E(\rho_2)$ and the logarithm of the mean squared wave number k^2 are well correlated. The correlations also indicate that the assumption of a Gaussian distribution of the densities is valid. Indeed the 30-year averaged entropy density functions are near-Gaussian, and only a few individual realizations differ markedly from Gaussian (not shown).

In Figure 4 we show the ρ_1-density functions for the six 10-day mean height fields shown in Figure 3. The low entropy cases have a compact uni-modal density and the high-entropy cases have a broad, in the middle almost flat density.

Next we examine if high or low entropies are associated with typical configurations of the 500 *mb* height field. For this purpose we constructed composite maps of atmospheric circulations with high and low entropies. Since the entropies exhibit annual cycles we calculated the composites for January and July months separately. We defined the high (low) composites as

the average of 10% of all atmospheric states with the highest (lowest) entropy for 10-day mean data (9 states of a total of 90 samples). The composites are presented in the form of absolute maps as well as anomalies by subtracting a "normal" defined as the mean of the middle third of all cases (33%-66% range in terms of the E-regime distribution).

For estimating the statistical stability of the composite anomaly map differences a (univariate) recurrence analysis (von Storch and Zwiers, 1988) was applied. This method compares two ensembles and establishes a measure of the strength of their discrimination. In our case one ensemble contains 9 atmospheric states with high (or low) entropy and the other ensemble contains 30 average-value entropy atmospheric states. At each grid point the distribution of the high (or low) entropy cases is compared with the distribution of the average-value entropy cases. The recurrence analysis results in the probability that a sample, which might belong to either the high (or low) entropy or the average-value entropy ensemble, will be classified correctly as a high (low) or average entropy case. A formal definition of this probability and the way it is estimated from the data is in Appendix C. An alternative, and more conventional statistical approach would have been to use a t-test. A shortcoming of this hypothesis testing approach is, however, the dependency of the result (i.e, rejection of the null hypothesis or not) on the sample size. The recurrence analysis delivers only estimates and makes no certain statements (such as "reject null hypothesis with a risk of less than 5%").

In the following we will deal mainly with composites of zonal (U_g) and meridional (V_g) components of the geostrophic wind derived from the 500 *mb* geopotential height field (Figs. 5 and 6, 8 and 9). To have an idea about the vertical structure of the high, or low entropy circulation we compare also composites of the 500 *mb* geopotential height and sea level pressure fields (Figure 7).

Figures 5 and 6 show January composites and composite anomalies of U_g and V_g calculated with entropy $E(\rho_1)$. Obviously the composite anomalies for both variables are not mirror images of each other. The "low − normal" difference of U_g (Figure 5a,d,e) is statistically weakly stable with moderate p-values $\leq$ 30%, whereas the high anomaly composite (Figure 5b,c) reveals a statistically strong and dynamically interesting pattern. It features an intensification of the jet stream over the western North Atlantic at $40°N$, with $p \geq 80\%$. Westerlies north of $50°N$ and

south of $30°N$ are weakened so that the core of the jet stream is narrower and steeper than in the "normal" state (Figure 5a). Horizontal gradients of U_g which play an important role for the development of barotropic instability (particularly the longitudinal gradient of U_g) are increased in the high entropy state. The low entropy flow is characterized by weak gradients (Figs. 5d and 6d): the anomalies of V_g (Figure 6e) tend to decrease the amplitude of V_g almost everywhere, with p-values $\leq 30\%$, and partly $\leq 20\%$, in the central North Atlantic. The high entropy anomaly composite of V_g (Figure 6c) has negative values, which are statistically stable with $p \leq 20\%$, over the northeast coast of North America and positive but less stable anomalies over eastern Europe. Thus the meridional circulation is weakened over these regions. Similarly to U_g, the high entropy composite of V_g possesses strong horizontal gradients which could contribute to barotropic instability of the flow (Figure 6b).

The circulation anomalies associated with the high and low entropy $E(\rho_1)$ shown in Figures 5 and 6 appear to be equivalent barotropic. As a confirmation Figure 7 displays anomaly composite maps of 500 mb geopotential height and sea level pressure for January. The positions of the anomalies approximately coincide in both fields. The same is valid for the entropy $E(\rho_2)$ and for July circulation, too (not shown).

The composite maps of U_g and V_g for the entropy $E(\rho_2)$ in January are shown in Figures 8 and 9. The low entropy anomaly composites are similar in many aspects to those calculated for the entropy $E(\rho_1)$. Particularly, the meridional circulation (V_g, Figure 9d,e) is less intensive than in the "average" entropy state, with p-values $\leq 20\%$ west of $20°N$ and $\geq 70\%$ at the Greenwich Meridian. The U_g anomaly composite reveals qualitatively the same pattern as in the $E(\rho_1)$-case, but is statistically more stable with $p \leq 10\%$ for negative anomalies north of $70°N$ and $p \geq 80\%$ in the belt at $50°N$ east of $30°W$. The atmospheric circulation with high entropy $E(\rho_2)$ deviates markedly from a zonal flow with two moderately stable ($p \leq 30\%$) U_g-minima, southwest of the Iberian Peninsula and over Central Europe, and a secondary maximum east of Ireland, which is however not stable (Figure 8b,c). The minimum southwest of Iberia is associated with a strong V_g-signal (Figure 9b,c). The mean northward circulation west of $30°W$ (Figure 9a) is intensified by more than 5 m/sec ($p \geq 20\%$) and the southward circulation east of $20°W$ is similarly accellerated.

Composite maps of U_g and V_g in July are similar for both entropies $E(\rho_1)$ and $E(\rho_2)$. Since low anomaly composites are not statistically stable we present in Figure 10 only high $E(\rho_1)$-entropy composites of U_g and V_g together with "normal" composites. The westerlies are intensified in the belt at $60°N$ near Greenwich and are weakened at $45°N$ west of Greenwich (Figure 10a-c). The V_g-anomalies (Figure 10e,f) are in phase with the mean meridional circulation (Figure 10d) so that the mean circulation is intensified during high entropy episodes. Both U_g and V_g anomalies indicate again that the circulation with high entropy deviates strongly from the zonal flow.

2.3.2 Results Obtained for the Northern Hemisphere

Almost all results presented above for the North Atlantic region hold also for the whole Northern Hemisphere. The annual cycles of $E(\rho_1)$ and $E(\rho_2)$ are opposite in phase. $E(\rho_1)$ is well correlated with the logarithm of the Northern Hemisphere enstrophy, and the $E(\rho_2)$ is correlated with the logarithm of the mean squared wave number, as is evidenced by the following table:

	$\langle ln(\eta), E(\rho_1)\rangle$	$\langle ln(k^2), E(\rho_2)\rangle$
daily	0.88	0.72
10-day means	0.98	0.75

The mean annual correlations of both entropies are 0.67 for 10-day means and 0.47 for daily data.

Many features of the composite maps of U_g and V_g in the NAWE region reappear in the Northern Hemisphere analysis. Particularly, composite maps of zonal wind in January indicate an intensification of jet streams over the western parts of both oceans for high $E(\rho_1)$-entropy states (Figure 11). The signal is stronger in the North Pacific sector, with $p \leq 10\%$ for negative anomalies and $p \geq 80\%$ for positive wind anomalies, than in the North Atlantic. Westerlies in the low $E(\rho_1)$-entropy composite are slightly weaker and more uniformly distributed. However, the low anomaly composite of U_g is not stable in the North Pacific sector and has only moderate p-values in the North Atlantic. The high entropy composites have also a more wavy structure

as revealed by V_g-composites (Figure 12). Particularly, over the East Pacific/North American region the amplitude of meridional circulation exceedes values of 10 m/sec whereas V_g in the low entropy composite (Figure 12d) differs little from that in the "average" composite (Figure 12a).

2.3.3 Interannual Variability and E-regimes

To have some idea about the interannual variability of the informational entropy we plotted in Figure 13 the time behavior of the entropy $E(\rho_1)$ computed for daily data for all 30 years in 1958-1987 for the NAWE region (Figure 13a) and for the whole Northern Hemisphere (Figure 13b). The climatological annual cycle (the first two annual harmonics) was subtracted from the entropy. The first apparent feature is the abrupt increase of the entropy in 1960-1962 which might be related to the changes in the analysis procedure. After that period a slight decreasing trend of the entropy is noticeable. The interannual variability is not strong and is much weaker than daily variability, especially in the NAWE region (Figure 13a).

Finally we present E-regime distribution functions $\int_{-\infty}^{E} \rho_E(e)de$ for the NAWE region. Figure 14 shows E-distribution functions computed for daily $E = E(\rho_1)$ and $E = E(\rho_2)$ in January and July, together with fitted standard normal distributions. For the entropy $E(\rho_1)$ (Figure 14a) the curve corresponding to January is situated to the right of the July curve since the entropy $E(\rho_1)$ is generally smaller in summer than in winter (Figure 1). For the entropy $E(\rho_2)$ (Figure 14b) the opposite is true. Both curves for July daily data are slightly steeper than the January curves. It would imply that the corresponding density functions are narrower in summer and wider in winter. This means that in winter the structure of atmospheric circulation states characterized by its entropy can differ from its mean state more strongly than in summer.

Only the $E(\rho_1)$-distribution function derived from the ensemble of daily January vorticity fields is inconsistent with the assumption of normality; there are more low extremes than expected, and fewer high extremes.

2.4 Discussion

A major purpose of the informational entropy analysis is the classification of circulation regimes associated with different entropy extremes. In the previous section we have shown that there

are statistically stable differences between atmospheric states with high and low entropies in the North Atlantic / Western Europe regions and in the Northern Hemisphere. However, it is not possible to classify synoptical atmospheric states uniquely in terms of informational entropy. Particularly, the theoretical absolute minimum of entropy is attained for a zonal flow with constant $\xi = \xi_0$. The density function $\rho(r)$ is in this case a δ-function with zero values for all r except $r = \xi_0$. Zonal flows of different kinetic energy and with different enstrophy are indistinguishable from the point of view of informational entropy (in terms of $E(\rho_2)$). Obviously, the same can be valid for other types of circulation regimes.

Depending on our point of view we may see this disabilty as an advantage or as a disadvantage. If we think of our entropy measures as a tool to reproduce the synoptically defined classification in the sense of "grosswetterlagen" then we have not met our goal. However, in the following section we will show that the entropy measures $E(\rho_1)$ and $E(\rho_2)$ are related to some stability parameters of the quasibarotropic circulation. So that if we think of our entropy measures as a tool to map the stability properties of the phase space, then we might find synoptically very different states to be similar in their stability properties. In that sense, our instrument "entropy" is successful in identifying the synoptically invisible but dynamically relevant similarity in stability.

3 Stability Characteristics of Nonstationary Solutions of the Barotropic Equation

In this section we consider the stability of nonstationary solutions of the barotropic vorticity equation on a sphere (1). In Subsection 3.1 we introduce the notion of a *Local Instantaneous Lyapunov Exponent*, which is identical to the *Schmidt number* introduced by Navarra (1993) and Betti and Navarra (1993). In Subsection 3.2 we derive these exponents for solutions of the barotropic vorticity equation (1) under a condition that the forcing term on the right side does not depend on time. Another approach to the stability of stationary solutions for one particular case is presented in Subsection 3.3.

3.1 Definition of Local Instantaneous Lyapunov Exponents

Consider an autonomous dynamic system with an evolution operator or, in Navarra's terminology, the propagator $\mathcal{B}_{\Delta t}$:

$$\xi(t+\Delta t) = \mathcal{B}_{\Delta t}(\xi(t)). \tag{9}$$

Linearization of (9) yields an equation for a small disturbance ξ' from the solution of the equation (9) on time interval $(t, t+\Delta t)$

$$\xi'(t+\Delta t) = \left[\mathcal{B}^L_{\Delta t}(t)\right] \xi'(t) \tag{10}$$

with a linear operator $\mathcal{B}^L_{\Delta t}(t) = \frac{\partial \mathcal{B}_{\Delta t}}{\partial \xi}\Big|_{\xi=\xi(t)}$.

According to the *Multiplicative Ergodic Theorem* of Oseledets (1968) Lyapunov exponents can be evaluated as eigenvalues of a limit matrix, the existence of which can be proven under the condition of the existence of an invariant measure. To do so, we introduce the notation

$$\mathcal{M}_n = \prod_{k=-n}^{n} \mathcal{B}^L_{\Delta t}(t+k\Delta t). \tag{11}$$

Lyapunov exponents are given by

$$\lambda = \frac{1}{\Delta t} ln \left(\mu \left[lim_{n\to\infty} [\mathcal{M}_n^* \mathcal{M}_n]^{\frac{1}{2n+1}}\right]\right) \tag{12}$$

with the symbol * representing the adjoint operator. The symbol $\mu[\mathcal{A}]$ represents an eigenvalue of the operator $\mathcal{A}$. The sum of positive Lyapunov exponents $\sum \lambda^+$ is equal to the Kolmogoroff-entropy (Pesin, 1977) so that the inverse of the sum of all positive λ's characterizes the mean predictability time of trajectories of the system (9). However, our main interest is not in an average measure of predictability. Instead we look for a measure of the stability of a given trajectory in a finite time interval $(t-n\Delta t, t+(n+1)\Delta t)$. Oseledet's theorem supplies us with a good basis for the definition of *local Lyapunov exponents*

$$\lambda[n,\xi] = \frac{1}{(2n+1)\Delta t} ln \left(\mu \left[\mathcal{M}_n^* \mathcal{M}_n\right]\right). \tag{13}$$

The *instantaneous* local Lyapunov exponents are obtained with $n = 0$

$$\lambda[0,\xi] = \frac{1}{\Delta t} ln(\mu \left[\mathcal{B}^L_{\Delta t}(t)^* \mathcal{B}^L_{\Delta t}(t)\right]). \tag{14}$$

Analogously to the concept of the mean predictability time, introduced above, we can define a characteristic time of divergence of two trajectories, which are at time t close to each other, as the inverse of the sum of positive instantaneous local Lyapunov exponents

$$L(\lambda^+, \xi(t)) = \sum_{\lambda>0} \lambda[0, \xi(t)]. \tag{15}$$

3.2 Lyapunov Exponents and the Barotropic Vorticity Equation

Now we formulate the problem of computing local Lyapunov exponents for the barotropic vorticity equation (1). We assume that the forcing term on the right side of (1) does not depend on time so that we deal with an autonomous system. After discretization of the time derivative and after linearizing the equation (1) on time interval $(t, t+\Delta t)$ around a solution $\bar{\xi} = \nabla^2\bar{\psi}$, a linear equation of the form (10) is obtained:

$$\xi'(t+\Delta t) = \left[1 - \Delta t\mathcal{A}(t) + O(\Delta t^2)\right] \xi'(t) \tag{16}$$

with the linear operator $[\mathcal{A}(t)]\,\xi' = J(\bar{\psi}, \xi') + J(\nabla^{-2}\xi', \bar{\xi} + f) + \alpha\xi' + \mu\nabla^4\xi'$. Since the forcing term under our assumptions is canceled in the linearized form of (1), the equation (16) describes the evolution of ξ' only due to internal dynamics and not due to external forcing.

For sufficiently small time steps Δt the instantaneous Lyapunov exponents are closely related to the eigenvalues of the operator $-(\mathcal{A} + \mathcal{A}^*)$:

$$\begin{aligned} &\mu\left[\mathcal{B}^L_{\Delta t}(t)^* \mathcal{B}^L_{\Delta t}(t)\right] = \\ &\quad = \mu\left[(1 - \Delta t\mathcal{A}^*)(1 - \Delta t\mathcal{A}) + O(\Delta t^2)\right] \\ &\quad \approx 1 - \Delta t\mu\left[\mathcal{A} + \mathcal{A}^*\right] + O(\Delta t^2). \end{aligned} \tag{17}$$

For sufficiently short times the instantaneous Lyapunov exponents (14) are approximately the eigenvalues of the symmetrical part of the operator $-\mathcal{A}$. Multiplying scalar (16) by itself we obtain

$$\begin{aligned} \eta'(t+\Delta t) = \eta'(t) - \Delta t\langle(\mathcal{A} + \mathcal{A}^*)\xi'(t), \xi'(t)\rangle \\ + O(\Delta t^2). \end{aligned} \tag{18}$$

Therefore, we can consider the eigenfunctions of the operator $-(\mathcal{A} + \mathcal{A}^*)$ with positive eigenvalues (i.e., positive Lyapunov exponents) as the directions along which the enstrophy η'

grows. *The sum of positive Lyapunov exponents, $L(\lambda^+, \xi)$, is the instantaneous growth rate of enstrophy for uniformly distributed disturbances of vorticity* along all unstable directions (see also Navarra (1993) and Betti and Navarra (1993)). We failed to relate theoretically the sum of the positive Lyapunov exponents to an overall measure such as enstrophy or mean squared wave number, even under very simplified circumstances. We will however see, in the next Section 4, that the observations allude to a relationship $L(\lambda^+, \xi) \sim E(\rho_1)$.

The sum of positive instantaneous Lyapunov exponents $L(\lambda^+, \xi)$ should only with reservations be interpreted as an instability measure of barotropic flow in terms of enstrophy growth. The assumption of uniformly distributed vorticity disturbances along all unstable directions and a zero amplitude of disturbances along stable directions at the initial time needed for such interpretation is rather dubious. A hope is that after a certain time the unstable modes will dominate the evolution of vorticity disturbances and, consequently, will define the growth of enstrophy. However, problems still remain with the requirement of equal amplitudes of vorticity projections onto unstable modes. Instead of the sum of all positive Lyapunov exponents we can use the largest instantaneous Lyapunov exponent for the most unstable direction as a measure of instability. In any case, either the sum of positive Lyapunov exponents or the largest Lyapunov exponent can provide at best a very crude measure of instability of the atmospheric flow. Moreover, they take into account only barotropic effects and do not provide the possibility of baroclinic instability.

The stability of a barotropic flow can also be measured by the rate of growth of kinetic energy. To do so we apply the operator ∇^{-2} to both sides of (16) and multiply it scalar by (16) itself getting

$$|K|'(t+\Delta t) = |K|'(t) + O(\Delta t^2) + \Delta t\langle(\mathcal{A}\nabla^2 + \nabla^2\mathcal{A}^*)\psi', \psi'\rangle \tag{19}$$

where $|K|'(t) = \langle\nabla\psi'(t), \nabla\psi'(t)\rangle$ is the kinetic energy of disturbance ψ' at time t. Therefore *the sum $K(\lambda^+, \xi)$ of positive eigenvalues of the operator $(\mathcal{A}\nabla^2 + \nabla^2\mathcal{A}^*)$ is the mean instantaneous growth rate of the kinetic energy for uniformly distributed disturbances of streamfunction* and can also be interpreted as a measure of instability. The problems with such interpretation are the

same as for $L(\lambda^+, \xi)$, the only differences being that the requirement for uniformly distributed vorticity disturbances along unstable directions is replaced by a requirement for streamfunction disturbances, and that the unstable directions for kinetic energy differ from these for enstrophy.

In the next section the analysis of observed fields will disclose that the two measures of stability, $L(\lambda^+, \xi)$ and $K(\lambda^+, \xi)$, are practically identical. The last one is, under certain simplifying circumstances, theoretically related to the enstrophy η. The mathematics of this exercise are presented in Appendix D. First, it is shown that the operator $\mathcal{A}\nabla^2 + \nabla^2\mathcal{A}^*$ has a symmetric spectrum of eigenvalues so that the sum of positive eigenvalues of this operator is monotonically related to the sum of all squared eigenvalues. Finally, it is proven that the sum of all squared eigenvalues of the operator $\mathcal{A}\nabla^2 + \nabla^2\mathcal{A}^*$ is related to the enstrophy of the flow.

3.3 k^2 as a Measure of Stability

Earlier we found, in an analysis of observed data as well as in a simplified dynamical framework that the entropy $E(\rho_2)$ is strongly related to the squared wavenumber k^2. On the other hand, the $E(\rho_2)$ was found to be related only moderately to $E(\rho_1)$ which in turn is strongly related to the Lyapunov-type stability measures. So, $E(\rho_2)$ cannot stand for the Lyapunov-type stability but must, at least in part, represent another dynamical aspect of the instantaneous flow field ξ. Here, we offer two candidates:

- If the Jacobian term in (1) is much smaller than all other terms, then quasi-stationarity of the flow field requires an approximate compensation of diffusion and forcing. (There are some observational indications (Holopainen and Fortelius, 1986) that such a compensation can occur during blocking events which have equivalent barotropic structure and can be considered in the first approximation as quasistationary solutions of (1)). In that particular case Dymnikov's et al (1990) I_3-index

$$I_3(\bar{\psi}) = -\frac{\eta}{|K|} - \frac{2\Omega}{a^2}\frac{|M|}{|K|}. \tag{20}$$

  is a stability measure (for the details, see Appendix E). The first term in (20) is by definition k^2. The second one is proportional to the ratio of mean angular momentum $|M|$ to kinetic energy $|K|$. The physical meaning of the index (20) is: stationary solutions

of (1), under the aforementioned conditions, are more stable if they are, under otherwise identical conditions, of larger scale (smaller k^2) and possess a smaller angular momentum. In the following section we will see that k^2 is the main contributer to the variation of the instability index I_3 so that we can use k^2 as a stability measure of such regimes instead of I_3.

- The squared wavenumber k^2 can be considered in some sense to be a measure of persistence, on the assumption that fluctuations of smaller space scales will have generally shorter lifetimes: baroclinic waves have time scales of less than a week compared to planetary quasi-barotropic waves with time scales of several weeks. To quantify this idea we fitted first-order autoregressive processes to the spectral coefficients of 10-day means of 500 mb geopotential height. If the autoregressive coefficient is labelled a then $\frac{1+a}{1-a}$ is a measure of persistence. The results of these calculations indicate that, for fluctuations with smaller wave numbers ($k = 1$ to 3) or of larger space scale, the autoregressive coefficient a is slightly less than unity (higher persistence); for higher wavenumbers, though, a becomes smaller. Admittedly, this is just a rough and ready check but it supports our notion that k^2 can be interpreted as a stability measure, in the sense of *persistence* of atmospheric regimes.

4 Correlation between Informational Entropy and the Stability Measure

In this section we examine the relationship between our various measures of (barotropic) stability:

- the informational entropy $E(\rho_1)$ (which was shown to be strongly related to the enstrophy), and the informational entropy $E(\rho_2)$ (which was found to be correlated with the squared wave number),

- the largest instantaneous local Lyapunov exponent,

- the sum of positive Lyapunov exponents $L(\lambda^+, \xi)$ (i.e., the sum of all positive eigenvalues of the operator $-(\mathcal{A} + \mathcal{A}^*)$) (which was shown in the preceeding section to describe the growth of enstrophy),

- the sum $K(\lambda^+, \xi)$ of all positive eigenvalues of the operator $\mathcal{A}\nabla^2 + \nabla^2 A^*$ (which was shown in the previous section to describe the growth of kinetic energy),

- the instability index I_3 (20).

For this purpose, we approximated for each 10-day mean of the 30 year data set the operator $\mathcal{A}$ in the "T21"-space of spherical harmonics with a triangular truncation at wave number 21. The linear drag coefficient α is set to $\frac{1}{7days}$ and the horizontal diffusion coefficient μ is equivalent to an e-folding time of 1.12 days for spherical harmonics with the highest wave number. The basic state of relative vorticity was derived from the Northern Hemisphere geopotential height field. The instability index I_3 was evaluated for both the Northern Hemisphere and the NAWE region.

We calculated for each of the 30 years 1958 through 1987 the correlations for various pairs of stability measures.

- $L(\lambda^+, \xi)$ and $K(\lambda^+, \xi)$ have mean correlation > 0.995.

- The sum $L(\lambda^+, \xi)$ of positive instantaneous Lyapunov exponents is well related to the informational entropy $E(\rho_1)$ with a mean annual correlation of 0.84 (minimum of about 0.55, maximum of 0.95).

- The largest positive instantaneous local Lyapunov exponent and $E(\rho_1)$ are less well related than $L(\lambda^+, \xi)$ and $E(\rho_1)$: The mean correlation is 0.63, with a minimum of 0.23 and a maximum of 0.80. That the correlation for the sum of Lyapunov exponents is higher than the correlation for the maximum Lyapunov exponent implies that the growth of the enstrophy in all unstable directions is better related to the structure of the flow measured in terms of entropy $E(\rho_1)$.

- The correlation between $L(\lambda^+, \xi)$ and $E(\rho_2)$ is lower (0.46 for 10-day means).

- The instability index I_3 and the mean squared wave number k^2 calculated for the NAWE region are well correlated with a mean annual correlation of 0.83. Consequently, k^2 is the main term in the variability of I_3. The mean annual correlation between I_3 and $E(\rho_2)$ computed for the same region is 0.77.

  For the Northern Hemisphere the mean annual correlations between I_3 and k^2 as well as between I_3 and $E(\rho_2)$ are smaller (0.67 and 0.43).

We may conclude: *Both Lyapunov-type measures $L(\lambda^+, \xi)$ and $K(\lambda^+, \xi)$ represent the same information, and are well related to the entropy $E(\rho_1)$.* This result is reasonable in the light of our theoretical findings, $E(\rho_1) \sim \eta$ and $K(\lambda^+, \xi) \sim \eta$ (which required some simplifications in the Appendices A and D). The next point we can make is: *The entropy measure $E(\rho_2)$ calculated for the NAWE region is well related to the instability index index I_3.* However, $E(\rho_2)$ computed for the Northern Hemisphere is not a useful approximation of any of the dynamically defined measures.

The notion of entropy can be applied for a classification of atmospheric circulation regimes in any geographical region. However, a correct formulation of the problem of computing Lyapunov-type stability measures for barotropic circulation is easier for the global region. Dymnikov et al. (1990) proposed to define regional instability indices taking into account only those unstable eigenvectors which are localized in the region of study. This procedure seems to be suitable for instantaneous Lyapunov exponents since eigenvectors of the corresponding operator are strongly localized (not shown). One might hope that the localized eigenvectors and the corresponding eigenvalues depend mainly locally on the basic state.

The entropy $E(\rho_1)$ calculated for the NAWE region is only weakly related to the global $L(\lambda^+, \xi)$ with a mean annual correlation of 0.34. If we, however, use for computing $L(\lambda^+, \xi)$ only the eigenvectors whose norm over the NAWE region is larger than 35% of their norm over the whole Northern Hemisphere then the mean annual correlation becomes 0.46. We see that even for "localized" eigenvectors the relationship is still not strong. Nevertheless, the systematic increase of correlations was detected for each individual year, indicating that such an improvement of results is not just by chance.

5 Summary and Conclusions

The present paper makes an attempt to classify regimes of barotropic atmospheric circulation by means of the "informational entropy" of a given atmospheric state. Two different entropy densities are introduced. One density, $\rho_1(r)$, is formulated in terms of the size of sets of r such that $r = \xi(t)$ of the given vorticity field $\xi(t)$ at time t. The other definition ρ_2 is based on the relative vorticity normalized by the kinetic energy of the flow; this reduces all atmospheric states to an equal energy level and uses the portions of kinetic energy instead of the area.

Both entropy definitions possess usefull properties. Particularly, the entropy $E(\rho_2)$ characterizes only the spatial structure of the atmospheric state and is independent of its amplitude. It can be reasonable if we want to have the definition of the entropy which is a measure of system organization. Moreover, the entropy $E(\rho_2)$ in some situations can serve as a stability index, for example, for quasibarotropic atmospheric regimes with a strong compensation between the external forcing and the dissipation as occurs in certain types of blocking events. On the other hand, the entropy $E(\rho_1)$ contains information not only about the spatial structure of the atmospheric circulation but also about its strength. It was shown that for the barotropic motions the entropy $E(\rho_1)$ is related to the instantaneous local Lyapunov exponents which characterize in some sense the stability of the atmospheric circulation.

The complexity of the atmospheric state in the North Atlantic/Western Europe region was found to depend on the entropy: regimes with low entropy exhibit only weak patterns whereas high entropy states go with complex structures.

By means of entropy we introduced the notion of E-regimes, and we defined a probabilistic measure for atmospheric regimes as being the time that the atmospheric system spends in states with the entropy within the interval $(E, E+dE)$. Defined in such a way, the distribution function of E-regimes can be used for the verification of climatic models.

A major finding of this paper is the close relationship between entropy and stability characteristics of atmospheric quasibarotropic circulation. The entropy $E(\rho_1)$ relates very well to both the sum of positive instantaneous Lyapunov exponents which characterizes the growth rate of disturbance enstrophy, as well as to the sum of positive eigenvalues of the operator in the equation for disturbances of barotropic kinetic energy which describes the growth rate of

disturbance kinetic energy. The last characteristic of stability was shown theoretically to be related to the enstrophy of the basic state. Therefore we can consider the E-regime distribution function in some sense as a distribution of regimes in terms of their dynamical stability. Similar interpretation is possible for the entropy $E(\rho_2)$. But in this case the stability is measured by the instability index I_3 which can be applied to certain types of stationary regimes. Note that the aim of the present paper was not to discuss in details the proporties of stability indices considered in this study. Numerious studies (e.g. Frederiksen and Frederiksen, 1993 and references therin) indicate that such gross measures of instability are not substitute for doing the instability calculations.

The calculation of the dynamical stability measures, in particular the Lyapunov-type measures L and K, requires some mathematical and computational investment of effort. For limited areas within the extratropics these dynamical measures are not well defined. Therefore, the entropy measures may serve as a cheap alternative to the more sophisticated approaches.

6 Acknowledgments

A large part of this work was undertaken at the Max-Planck-Institute for Meteorology in Hamburg (FRG) during several visits to this institute by Valentin Dymnikov who was supported by the Max-Planck Society. Viacheslav Kharin and Hans von Storch enjoyed fruitful discussions with Antonio Navarra. Jorgen S. Frederiksen helped us with valuable comments. Valentin Dymnikov thanks Eugene Kazantsev. The data set was prepared by Ingo Jessel. We wish to thank Marion Grunnert who thoroughly prepared the diagrams.

Appendices

A Entropy $E(\rho_1)$ and the Logarithm of the Enstrophy

A Gaussian entropy density function ${\rho_1}^{\xi(t)}$ of a vorticity field $\xi(t)$ at a time t may be written as

$$ {\rho_1}^{\xi}(r) = \frac{1}{\sqrt{2\pi\sigma^2}} \exp\left[-\frac{(r-\mu)^2}{2\sigma^2}\right]. \tag{21} $$

Here r is any possible value of relative vorticity in the real domain, μ and σ^2 are the mean value and the standard deviation respectively of the density ${\rho_1}^{\xi}$. Because of the way the density is defined, μ and σ^2 are also the spatial mean and the spatial variance of the considered vorticity field $\xi(t)$.

For enstrophy we have by definition

$$ \begin{aligned} \eta &= \frac{1}{|D|}\int_D \xi^2(x)dx = \int_{v(D)} r^2\rho_1(r)dr \\ &= \int_{-\infty}^{\infty} r^2\rho_1(r)dr = \sigma^2 + \mu^2. \end{aligned} \tag{22} $$

The entropy, on the other hand, is

$$ \begin{aligned} E(\rho_1) &= -\int_{-\infty}^{\infty}\rho_1(r)ln(\rho_1(r))dr \\ &= \int_{-\infty}^{\infty}\rho_1(r)\left(ln\sqrt{2\pi\sigma^2} + \frac{(r-\mu)^2}{2\sigma^2}\right)dr \\ &= ln\sqrt{2\pi\sigma^2} + \frac{1}{2\sigma^2}\int(r-\mu)^2\rho_1(r)dr \\ &= \frac{1}{2}ln(\eta - \mu^2) + \text{constant}. \end{aligned} \tag{23} $$

In the course of calculations we have used (21) and (22). (23) shows that if $\mu = 0$, which is true for the global region and with a good approximation for the NAWE region, the entropy $E({\rho_1}^{\xi}(t))$ is a linear function of the logarithm of enstrophy $\eta(\xi(t))$.

How does the entropy change if the vorticity field is multiplied by a constant c? With (23) we may write

$$ \begin{aligned} E({\rho_1}^{c\xi}) &= \frac{1}{2}ln\left(\eta(c\xi) - \mu(c\xi)\right) + \text{constant} \\ &= \frac{1}{2}ln\left(c^2(\eta(\xi) - \mu(\xi))\right) + \text{constant} \\ &= E({\rho_1}^{\xi}) + ln(c). \end{aligned} $$

The last term, $ln(c)$, is positive for $c > 1$ and negative for $c < 1$ so that $E(\rho_1)$ varies monotonically with the "amplitude" c.

B Entropy $E(\rho_2)$ and the Mean Squared Wave Number

In this Appendix we again assume the entropy density function $\rho_2{}^{\xi}(r^*)$ to be Gaussian (21). Applications of the definition (8), of (22) and of $r^* = r/\sqrt{|K|}$ (with any possible vorticity value r which might be contained by the field ξ or not) lead to

$$\begin{aligned} \sigma^2 + \mu^{*2} &= \int_{-\infty}^{\infty} r^{*2} \rho_2(r^*) dr^* \\ &= \frac{1}{|K|^2} \int_{-\infty}^{\infty} r^2 dK \\ &= \frac{\eta}{|K|} \frac{\frac{1}{|K|}\int r^2 dK}{\frac{1}{D}\int r^2 dx} = k^2 R \end{aligned} \tag{24}$$

where $\mu^{*2} = \mu^2/|K|$. R is the ratio of the squared relative vorticity integrated over the kinetic energy to the squared relative vorticity integrated over the region area. In the 30-year data set of daily vorticity field ξ we have found a correlation of 0.98 between k^2 and $k^2 R$ so that we may identify $Rk^2 \sim k^2$.

For the entropy $E(\rho_2)$ we find:

$$\begin{aligned} E(\rho_2) &= \int_{-\infty}^{\infty} \rho_2(r^*)(ln\sqrt{2\pi\sigma^2} + \frac{(r^* - \mu^*)^2}{2\sigma^2}) dr^* \\ &= \frac{1}{2} ln(k^2 - \mu^{*2}) + \text{constant}. \end{aligned} \tag{25}$$

If $\mu^* = 0$, which is true with a good approximation, then (25) is the desired linear relationship between entropy $E(\rho_2)$ and the logarithm of the squared wave number $k^2(\xi(t))$.

Finally we show that two fields with the same pattern but different amplitudes have the same entropy $E(\rho_2)$:

$$\begin{aligned} E(\rho_2{}^{c\xi}) &= \frac{1}{2} ln \frac{\eta(c\xi) - \mu^2(c\xi)}{|K|(c\xi)} + \text{constant} \\ &= \frac{1}{2} ln \frac{c^2(\eta(\xi) - \mu^2(\xi))}{c^2|K|(\xi)} + \text{constant} \\ &= E(\rho_2{}^{\xi}). \end{aligned}$$

C Recurrence Analysis

In the "Recurrence Analysis" (von Storch and Zwiers, 1988) two random variables $\mathbf{X}$ and $\mathbf{Y}$, with expectations μ_X and μ_Y, are compared by calculating the probability

$$prob\,(\mathbf{Y} > \mu_X) = 1 - prob\,(\mathbf{Y} < \mu_X) = p \tag{26}$$

If $p = 50\%$ then the random variables are not separated from each other. A large value such as $p = 95\%$ or a small value such as $p = 5\%$ indicates that the two random variables overlap only little. If $p = 95\%$ then any random realization of $\mathbf{Y}$ will very likely be larger than the mean of $\mathbf{X}$, and only 5% of all $\mathbf{Y}$-realizations will be smaller than this threshold. The opposite interpretation applies for $p = 5\%$.

If both random variables are Gaussian distributed with the same variance σ^2 then the probability p is given by

$$p = F_S^{-1}\left(\frac{\mu_X - \mu_Y}{\sigma^2}\right) \tag{27}$$

with the standard normal (cumulative) distribution function F_S. In practical situations, as in the present study, the estimated means and the estimated standard deviation are used for the computation of (27).

It should be noted that the level of recurrence, p, does not imply any statement on a statistical significance (like the rejection of the null hypothesis of equal means with a controlled certainty). Instead p is an *estimated measure of statistical stability.*

D Proof of $K(\lambda^+, \xi) \sim \eta(\xi)$

In this appendix we show, under significantly simplifying assumptions, that the eigenvalues of the operator

$$\mathcal{S} = \mathcal{A}\nabla^2 + \nabla^2\mathcal{A}^* \tag{28}$$

are symmetrically distributed around zero. $\mathcal{A}$ is the numerical representation of the linearized barotropic operator used in (16). The simplifying asumptions are

- The linear drag and the diffusion are set to zero ($\alpha = \mu = 0$ in (1)).

- The stationary solution $\bar{\xi}$ is zonally symmetric ($\bar{\xi} = \bar{\xi}(y)$).

Then $\mathcal{S}$ is of the form

$$\mathcal{S} = \bar{u}\frac{\partial}{\partial x}\nabla^2 - \nabla^2\left[\bar{u}\frac{\partial}{\partial x}\right] \tag{29}$$

with Cartesian coordinates x and y and $\bar{u} = \frac{\partial\bar{\psi}}{\partial y}$. To derive (29) we have used the fact that the expression $\mathcal{A}\nabla^2\psi$ may be split up into two Jacobians, one being symmetric and the other antisymmetric with respect to ψ'. When forming the sum (28) the antisymmetric term is cancelled.

After simple manipulations the operator $\mathcal{S}$ can be rewritten in the form

$$\mathcal{S} = \frac{\partial}{\partial x}\left[\frac{\partial}{\partial y}\bar{\xi} + \bar{\xi}\frac{\partial}{\partial y}\right]. \tag{30}$$

The eigenfunctions ϕ and eigenvalues λ of the operator $\mathcal{S}$ satisfy

$$\frac{\partial}{\partial x}\left[\frac{\partial\bar{\xi}\phi}{\partial y} + \bar{\xi}\frac{\partial\phi}{\partial y}\right] = \lambda\phi. \tag{31}$$

Since the mean flow $\bar{\xi}$ is independent of x we may search for solutions of the form $\phi(x,y) = \sum_m \tilde{\phi}_m(y)e^{imx}$. The equation for $\tilde{\phi}_m$ takes the form

$$\frac{\partial\bar{\xi}\tilde{\phi}_m}{\partial y} + \bar{\xi}\frac{\partial\tilde{\phi}_m}{\partial y} = \frac{\lambda}{im}\tilde{\phi}_m. \tag{32}$$

Thus $\tilde{\phi}_m$ is an eigenfunction of the operator on the left side of (32). This operator is skew-Hermitian and has purely imaginary, conjugate complex eigenvalues ν. Because $\lambda = im\nu$, all eigenvalues of the operator $\mathcal{S}$ are real and symmetric relative to zero, i.e., they are of the form $\lambda = \pm Imag(m\nu)$.

This symmetry property of the eigenvalues of the operator $\mathcal{S}$ allows us to study the spectrum of the operator $\mathcal{S}\mathcal{S}^* \equiv \mathcal{S}^2$ instead of $\mathcal{S}$. Indeed, we have in this case

$$\begin{aligned} K(\lambda^+,\bar{\xi}) &\equiv \sum\mu^+[\mathcal{S}] \sim \sum\mu^{+2}[\mathcal{S}] \\ &= \frac{1}{2}\sum_{all}\mu^2[\mathcal{S}] \equiv \frac{1}{2}Trace(\mathcal{S}^2). \end{aligned} \tag{33}$$

The sign $\sim$ in (33) stands for monotonic dependence. Let S be a matrix which approximates the operator $\mathcal{S}$. Then $Trace(\mathcal{S}^2)$ can be estimated by $\sum_{ij} {s_{ij}}^2$ with s_{ij} the elements of the matrix

S. If we discretize the operator $\mathcal{S}$ like

$$\begin{aligned}(\mathcal{S}\phi)_{ij} = \frac{1}{h_x h_y}(&\bar{\xi}_{i+1,j+\frac{1}{2}}\phi_{i+1,j+1} \\ &- \bar{\xi}_{i+1,j-\frac{1}{2}}\phi_{i+1,j-1} - \bar{\xi}_{i-1,j+\frac{1}{2}}\phi_{i-1,j+1} \\ &+ \bar{\xi}_{i-1,j-\frac{1}{2}}\phi_{i-1,j-1})\end{aligned} \tag{34}$$

then $\sum_{ij} {s_{ij}}^2 \sim \sum_{ij} \bar{\xi}_{ij}^2 \sim \eta(\bar{\xi})$. Thus we proved for this particular case that $K(\lambda^+, \bar{\xi}) \sim \eta(\bar{\xi})$.

E k^2 as a Measure of Stability

Let us consider stationary quasibarotropic atmospheric regimes with a full compensation between external forcing and internal dissipation (a more general case of regimes with a near full compensation between forcing and dissipation was considered by Dymnikov et al., 1990). Because of (1) the compensation is formally equivalent to

$$\alpha\nabla^2\psi + \mu\nabla^4\psi = F \tag{35}$$

and stationary solutions ψ (for the sake of brevity we omit the overbar which we have used in the main part of this paper to indicate a stationary solution) satisfy

$$J\left(\psi, \nabla^2\psi + f\right) = 0 \tag{36}$$

or, with some well-behaving function Φ:

$$\nabla^2\psi + f = \Phi(\psi). \tag{37}$$

Arnold's (1965) sufficient stability condition requires for all values of ψ in the region of study

$$\frac{\partial\Phi}{\partial\psi} > 0, \tag{38}$$

or,

$$\frac{1}{\mu_{min}[\nabla^{-2}]} < \frac{\partial\Phi}{\partial\psi} < 0 \tag{39}$$

where $\mu_{min}[\nabla^{-2}]$ is the minimal eigenvalue of the operator ∇^{-2} defined on a function space orthogonal to a constant. From (38) and (39) one can derive the necessary conditions for instability: either $\frac{\partial\Phi}{\partial\psi} = 0$ for at least one value of ψ, or $\frac{\partial\Phi}{\partial\psi} < 1/\mu_{min}[\nabla^{-2}]$. Thus we might

use the values of $\frac{\partial\Phi}{\partial\psi}$ for defining whether such atmospheric regimes would be stable or could be unstable. However, in most cases the analytical expression of Φ is unknown so that $\frac{\partial\Phi}{\partial\psi}$ cannot be calculated for a given observed field (which would satisfy the assumptions of compensation and stationarity only approximately in the best case). As a more practical alternative we introduce another measure which is much easier to compute while still closely related to $\frac{\partial\Phi}{\partial\psi}$. Multiplying scalar (37) by $\nabla^2\psi$ we get

$$\langle\Phi(\psi),\nabla^2\psi\rangle = \langle\nabla^2\psi,\nabla^2\psi\rangle + \langle f,\nabla^2\psi\rangle \tag{40}$$

On the other hand

$$\begin{aligned}\langle\Phi(\psi),\nabla^2\psi\rangle &= -\langle\nabla(\Phi(\psi)),\nabla\psi\rangle \\ &= -\langle\tfrac{\partial\Phi}{\partial\psi}\nabla\psi,\nabla\psi\rangle \\ &= -\frac{1}{|D|}\int\frac{\partial\Phi}{\partial\psi}|\nabla\psi|^2dx\end{aligned} \tag{41}$$

Dividing (40) by the kinetic energy $|K| = \frac{1}{|D|}\int|\nabla^2\psi|^2dx$ and taking into account (41) we have

$$\frac{\frac{1}{|D|}\int\frac{\partial\Phi}{\partial\psi}|\nabla\psi|^2dx}{\frac{1}{|D|}\int|\nabla\psi|^2dx} =$$

$$\begin{aligned}&= -\frac{\langle\nabla^2\psi,\nabla^2\psi\rangle}{|K|} - \frac{\langle f,\nabla^2\psi\rangle}{|K|} \\ &= -\frac{\eta}{|K|} - \frac{2\Omega}{a^2}\frac{|M|}{|K|}\end{aligned} \tag{42}$$

The first term on the right side of (42) is k^2 and the second one is proportional to the mean angular momentum $|M|$. The left side of (42), on the other hand, is the area mean of $\frac{\partial\Phi}{\partial\psi}$ weighted at each point by the kinetic energy of the basic state ψ and may be seen as a typical value of $\frac{\partial\Phi}{\partial\psi}$.

Dymnikov et al. (1990) called this value, with an opposite sign, an instability index I_3. They established a dependence between I_3 and the lifetime of North Atlantic blockings for which the hypotheses about quasistationarity and compensation were aproximately valid (Holopainen and Fortelius, 1986). They showed that the lifetime of blockings depends almost linearly on $-1/I_3$. Therefore this value may be a measure of stability of stationary solutions of (36).

References

Abarbanel H. D. I., Brown R, and Kennel M. B., 1991: Lyapunov exponents in chaotic systems: their importance and their evaluation using observed data. Int. J. Mod. Physics, B, 5, 1347-1375

Betti, A. and A. Navarra, 1993: On the prediction of the evolution of the variance in a barotropic model. J. Atmos. Sci. (submitted)

Blinova E. N., 1943: Hydrodynamical theory of pressure waves, temperature waves and atmospherical centers of action. Doklady Akademii Nauk SSSR, 39, N 7, 284-287, in Russian

Dymnikov V. P., 1990: Instability indices for quasi-stationary atmospheric regimes. Sov. J. Numer. Anal. Math. Modeling, 5, N 3, 189-198.

Dymnikov V. P. and Filatov A. N., 1990: The stability of large scale atmospheric processes. Gydrometeoizdat, Leningrad, 236 pp., in Russian

Dymnikov V. P., Kazantsev E. V. and Kharin V. V., 1990: The stability characteristics and lifetime of atmospheric circulation regimes. Izvestija AN, Fizika atmosfery i okeana. 26, N 4, 339-349, in Russian

Dymnikov V. P., Kazantsev E. V. and Kharin V. V., 1992: Informational entropy and local Lyapunov exponents of barotropic circulation. Izvestija AN, Fizika atmosfery i okeana. 28, N 6, 563-573, in Russian

Dymnikov V. P. and Skiba Ju. N., 1987: Barotropic instability of zonally asymmetric flows over topography. Sov. J. Numer. Anl. Math. Modelling, Holland, 3-18

Dzerdzeevsky B. N., 1956: Materials of meteorological investigations. Published by MGK of the Presidium of the USSR Academy of Sciences, in Russian

Frederiksen J. S. and Bell R. C., 1990: North Atlantic blocking during January 1979: Linear theory. Quart. J. Roy. Meteot. Soc., 116, 1289-1313

Frederiksen J. S. and Frederiksen C. S., 1993: Southern Hemisphere storm tracks, blockings, and low-frequency anomalies in a primitive equation model. J Atmos. Sci., 50, 3124-3163

Holopainen E. and Fortelius C., 1986: On the role of high frequency transient eddies in a blocking-type flow. J. Atmos. Sci., 44, 1632-1645

Kats A. L., 1960: The seasonal variations of the atmospheric general circulation and long range weather prediction. Gydrometeoizdat, Leningrad, 270 p., in Russian

Kurgansky M. V. and M. S. Tatarskaya, 1987: The potential vorticity concept in meteorology: A review. Izvestiya, Atmospheric and Oceanic Physics, 23, 587-606

Legras B., Desponts T. and Piquet B., 1989: Cluster analysis and weather regimes. Proceedings of ECMWF seminar on the nature and prediction of extratropical weather systems, 2, 123-149

Mo K. and Ghil M., 1987: Statistics and dynamics of persistent anomalies. J. Atmos. Sci. 44, 877-901

Molteni F., Tibaldi S. and Palmer T. N., 1990: Regimes in the wintertime circulation over northern extratropics. 1: Observational evidence. Quart. J. Roy. Meteor. Soc. 116, 31-67

Navarra, A., 1993: A new set of orthogonal modes for linearized meteorological problems. J. Atmos. Sci. 50, 2569-2583

Obukhov A. M, 1964: Adiabatic invariants for atmospheric processes. Meteorologija i gidrologija, 2, 3-9, in Russian

Oseledets V. I., 1968: Multiplicative ergodic theorem. Characteristical Lyapunov exponents of dynamic systems. Proceedings of Moscow Mathematical Society, 19, N 1, 179-210, in Russian

Pesin Ya. B., 1977: Characteristic Lyapunov exponents and smooth ergodic theory. Uspehi matematicheskih nauk, 32, N 1, 4-55, in Russian

von Storch H. and F. W. Zwiers, 1988: Recurrence Analysis of Climate Sensitivity Experiments. J. Climate, 1, 157-171

Figure Captions

Figure 1. The time behavior of the entropies $E(\rho_1)$ (top) and $E(\rho_2)$ (bottom) for the North Atlantic/Western Europe region in 1985 computed for daily data (upper solid line) and for 10-day means (lower solid line) together with the 1958-1987 mean annual cycles (dash lines) computed as the first two Fourier harmonics.

Figure 2. Scatter diagram of entropies $E(\rho_1)$ and $E(\rho_2)$ computed for all 10-day mean vorticity fields in the NAWE sector during winter (DJF). For the marked dots, the underlying 10-day mean geopotential height fields are shown in Figure 3.

Figure 3. Six 10-day mean geopotential height fields in the North Atlantic/Western Europe region. Each panel is labelled with the first day of its 10-day averaging interval. Also, the entropies $E(\rho_1)$ and $E(\rho_2)$ are added. The cases have been chosen with the help of Figure 2.
Left column: Low entropy cases.
a) 21 Dec. 1977, with minimum $E(\rho_1)$ and minimum $E(\rho_2)$.
b) 21 Jan. 1977, with third smallest $E(\rho_1)$ and second smallest $E(\rho_2)$.
c) 21 Feb. 1983, with low entropies $E(\rho_1)$ and $E(\rho_2)$.
Right column: High entropy cases.
d) 21 Dec. 1987, with maximum $E(\rho_1)$ and high $E(\rho_2)$.
e) 21 Feb. 1981, with high $E(\rho_1)$ and maximum $E(\rho_2)$.
f) 21 Dec. 1970, with high entropies $E(\rho_1)$ and $E(\rho_2)$.

Figure 4. The ρ_1-density functions of the three low-entropy cases (left) and high-entropy cases (right) shown in Figure 3.

Figure 5. Composites of geostrophic zonal wind U_g calculated from 10-day mean 500 *mb* geopotential height fields in January based on the entropy $E(\rho_1)$.
a) The mean of 30 "average" cases (the 33% - 66 %-range of E-regimes). Contour interval: 5 m/sec.

b,d) Average of the 9 cases with maximum (b, left column) and minimum (d, right) entropy $E(\rho_1)$ (or, mean of the upper (b) or lower (d) 10% of the E-regime distribution function). Contour interval: 5 $m/sec.$

c,e) Difference of the mean of 9 cases with maximum (c, left column) or minimum (e, right) entropy $E(\rho_1)$ and the mean of 30 "average" cases (a). Contour interval: $2m/sec.$ Stippling represents areas with estimated local level of recurrence $p \leq 30\%$ or $p \geq 70\%$ (light), $p \leq 20\%$ or $p \geq 80\%$ (moderate) and $p \leq 10\%$ or $p \geq 90\%$ (heavy).

Figure 6. Composites of geostrophic meridional wind V_g calculated from 10-day mean 500 mb geopotential height fields in January based on the entropy $E(\rho_1)$.

a) The mean of 30 "average" cases. Contour interval: 2 $m/sec.$

b,d) Average of the 9 cases with maximum (b) and minimum (d) entropy $E(\rho_1)$. Contour interval: 2 $m/sec.$

c,e) Difference of the mean of 9 cases with maximum (b) or minimum (d) entropy $E(\rho_1)$ and the mean of 30 "average" cases (a). Contour interval: 1 $m/sec.$ Stippling represents areas with estimated local level of recurrence $p \leq 30\%$ or $p \geq 70\%$ (light), $p \leq 20\%$ or $p \geq 80\%$ (moderate) and $p \leq 10\%$ or $p \geq 90\%$ (heavy).

Figure 7. Differences of composite for 500 mb height (a,c; contour interval: 20 gpm) and sea-level pressure (b,d; contour interval: 1 mb) calculated with the entropy $E(\rho_1)$. Stippling represents areas with estimated local level of recurrence $p \leq 30\%$ or $p \geq 70\%$ (light), $p \leq 20\%$ or $p \geq 80\%$ (moderate) and $p \leq 10\%$ or $p \geq 90\%$ (heavy).

a,b) Differences of the mean of the 10 day means with largest entropy $E(\rho_1)$ and the mean of 30 "average" cases (the 33% - 66 %-range of E-regimes).

b,d) Same as (a,c) but for minimum $E(\rho_1)$.

Figure 8. Same as Figure 5 but for entropy $E(\rho_2)$: Composites of geostrophic zonal wind U_g calculated from 10-day mean 500 mb geopotential height fields in January.

a) The mean of 30 "average" cases. Contour interval: 5 $m/sec.$

b,d) Average of the 9 cases with maximum (b) and minimum (d) entropy $E(\rho_2)$. Contour

interval: 5 m/sec.

c,e) Difference of the mean of 9 cases with maximum (c) or minimum (e) entropy $E(\rho_2)$ and the mean of 30 "average" cases (a). Contour interval: 2 m/sec. Stippling represents areas with estimated local level of recurrence $p \leq 30\%$ or $p \geq 70\%$ (light), $p \leq 20\%$ or $p \geq 80\%$ (moderate) and $p \leq 10\%$ or $p \geq 90\%$ (heavy).

Figure 9. Same as Figure 6 but for entropy $E(\rho_2)$: Composites of geostrophic zonal wind U_g calculated from 10-day mean 500 mb geopotential height fields in January.

a) The mean of 30 "average" cases. Contour interval: 2 m/sec.

b,d) Average of the 9 cases with maximum (b) and minimum (d) entropy $E(\rho_2)$. Contour interval: 2 m/sec.

c,e) Difference of the mean of 9 cases with maximum (c) or minimum (e) entropy $E(\rho_2)$ and the mean of 30 "average" cases (a). Contour interval: 1 m/sec. Stippling represents areas with estimated local level of recurrence $p \leq 30\%$ or $p \geq 70\%$ (light), $p \leq 20\%$ or $p \geq 80\%$ (moderate) and $p \leq 10\%$ or $p \geq 90\%$ (heavy).

Figure 10. "Average" and high $E(\rho_1)$-entropy composites of geostrophic zonal U_g (a-c; left column) and meridional wind V_g (d-f, right column) calculated from 10-day mean 500 mb geopotential height fields in July.

a,d) The mean of 30 "average" cases for U_g (a; contour interval: 5 m/sec) and for V_g (d; contour interval: 2 m/sec).

b,e) Average of the 9 cases with maximum entropy $E(\rho_1)$ for U_g (b; contour interval: 5 m/sec) and for V_g (e; contour interval: 2 m/sec).

c,f) Difference of the mean of 9 cases with maximum entropy $E(\rho_1)$ (b or e) and the mean of 30 "average" cases (a or d) for U_g (c; contour interval: 2 m/sec) and for V_g (f; contour interval: 1 m/sec). Stippling represents areas with estimated local level of recurrence $p \leq 30\%$ or $p \geq 70\%$ (light), $p \leq 20\%$ or $p \geq 80\%$ (moderate) and $p \leq 10\%$ or $p \geq 90\%$ (heavy).

Figure 11. Same as Figure 5 but for the Northern Hemisphere: Composites of geostrophic zonal wind U_g calculated from 10-day mean 500 mb geopotential height fields in January based

on the entropy $E(\rho_1)$.

a) The mean of 30 "average" cases. Contour interval: 5 $m/sec.$

b,d) Average of the 9 cases with maximum (b, left column) and minimum (d, right) entropy $E(\rho_1)$. Contour interval: 5 $m/sec.$

c,e) Difference of the mean of 9 cases with maximum (c, left column) or minimum (e, right) entropy $E(\rho_1)$ and the mean of 30 "average" cases (a). Contour interval: 2 $m/sec.$ Stippling represents areas with estimated local level of recurrence $p \leq 30\%$ or $p \geq 70\%$ (light), $p \leq 20\%$ or $p \geq 80\%$ (moderate) and $p \leq 10\%$ or $p \geq 90\%$ (heavy).

Figure 12. Same as Figure 5 but for the Northern Hemisphere: Composites of geostrophic meridional wind V_g calculated from 10-day mean 500 mb geopotential height fields in January based on the entropy $E(\rho_1)$.

a) The mean of 30 "average" cases. Contour interval: 2 $m/sec.$

b,d) Average of the 9 cases with maximum (b) and minimum (d) entropy $E(\rho_1)$. Contour interval: 2 $m/sec.$

c,e) Difference of the mean of 9 cases with maximum (b) or minimum (d) entropy $E(\rho_1)$ and the mean of 30 "average" cases (a). Contour interval: 1 $m/sec.$ Stippling represents areas with estimated local level of recurrence $p \leq 30\%$ or $p \geq 70\%$ (light), $p \leq 20\%$ or $p \geq 80\%$ (moderate) and $p \leq 10\%$ or $p \geq 90\%$ (heavy).

Figure 13. The time behavior of the entropy $E(\rho_1)$ computed for daily data for all 30 years in 1958-1987 for the NAWE region (a) and for the Northern Hemisphere (b). The first two climatological annual harmonics were subtracted from the entropy.

Figure 14. Daily E-regime distribution functions for $E = E(\rho_1)$ (top) and $E = E(\rho_2)$ (bottom) for January and July. Fitted standard normal distributions are added to the empirically derived distribution functions.

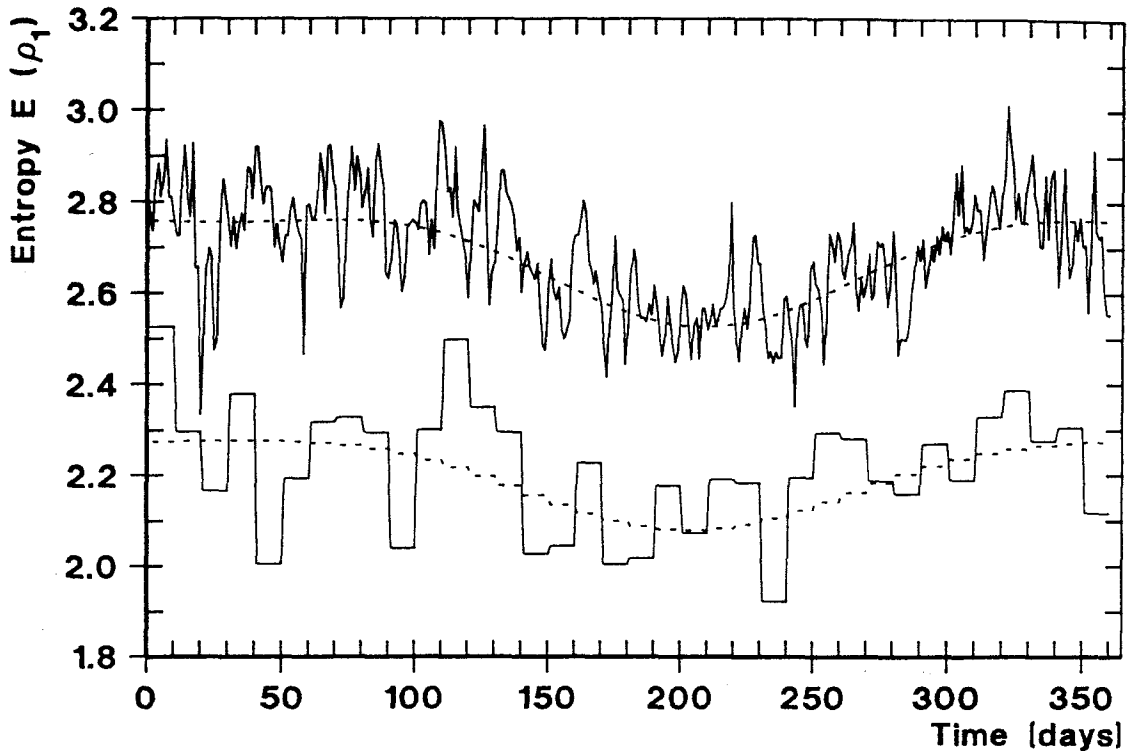
Entropy E (ρ_1)
3.2
3.0
2.8
2.6
2.4
2.2
2.0
1.8
0
50
100
150
200
250
300
350
Time [days]

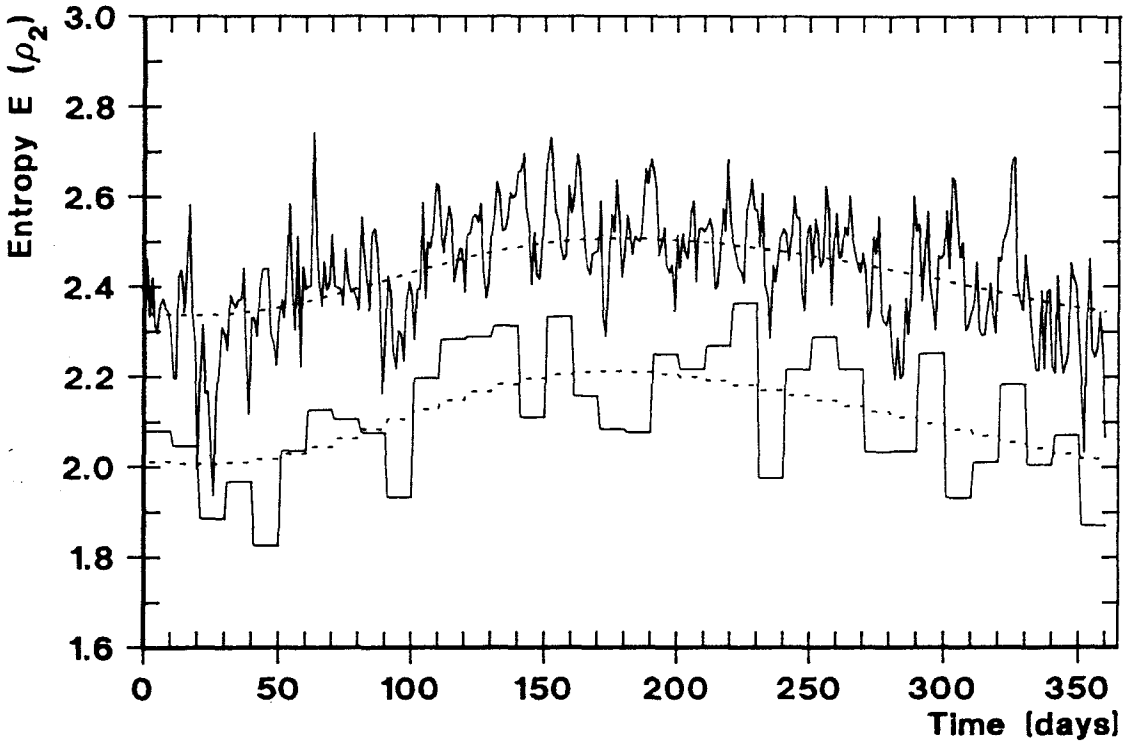
Entropy E (ρ_2)
3.0
2.8
2.6
2.4
2.2
2.0
1.8
1.6
0
50
100
150
200
250
300
350
Time [days]

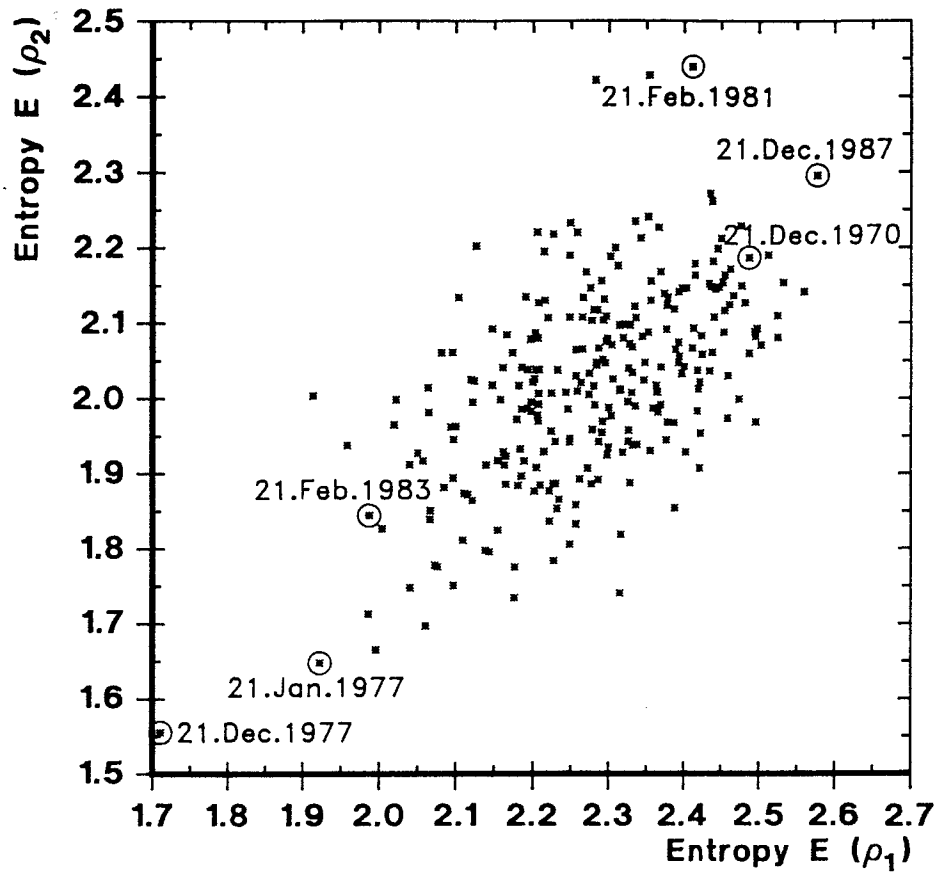
Entropy E (ρ_2)
2.5
2.4
2.3
2.2
2.1
2.0
1.9
1.8
1.7
1.6
1.5
21.Feb.1981
21.Dec.1987
21.Dec.1970
21.Feb.1983
21.Jan.1977
21.Dec.1977
1.7
1.8
1.9
2.0
2.1
2.2
2.3
2.4
2.5
2.6
2.7
Entropy E (ρ_1)

113SLKb

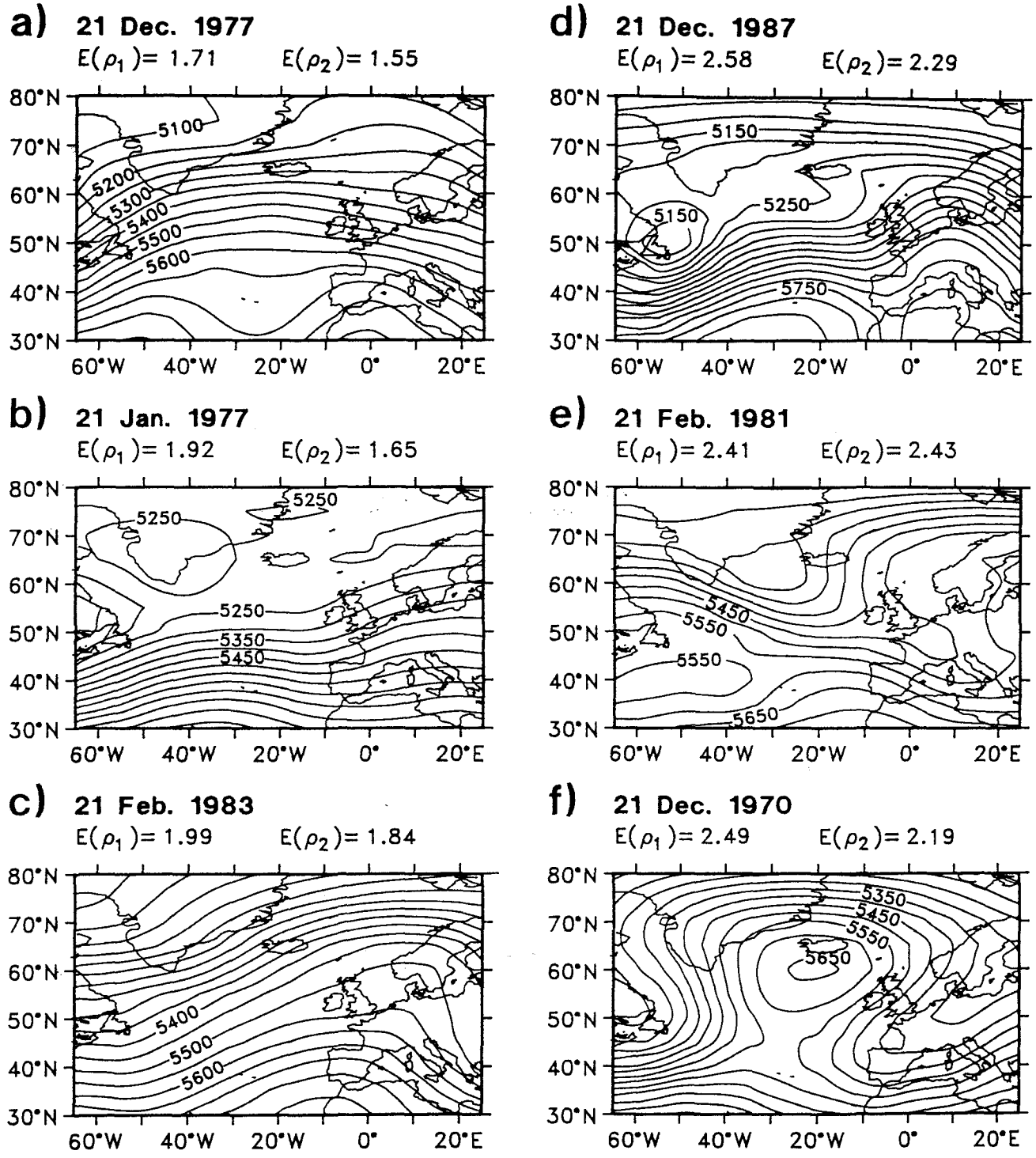
a) 21 Dec. 1977
E(ρ1)= 1.71
E(ρ2)= 1.55
5100
5200
5300
5400
5500
5600
b) 21 Jan. 1977
E(ρ1)= 1.92
E(ρ2)= 1.65
5250
5250
5250
5350
5450
c) 21 Feb. 1983
E(ρ1)= 1.99
E(ρ2)= 1.84
5400
5500
5600
d) 21 Dec. 1987
E(ρ1)= 2.58
E(ρ2)= 2.29
5150
5150
5250
5750
e) 21 Feb. 1981
E(ρ1)= 2.41
E(ρ2)= 2.43
5450
5550
5550
5650
f) 21 Dec. 1970
E(ρ1)= 2.49
E(ρ2)= 2.19
5350
5450
5550
5650
80°N
70°N
60°N
50°N
40°N
30°N
60°W
40°W
20°W
0°
20°E

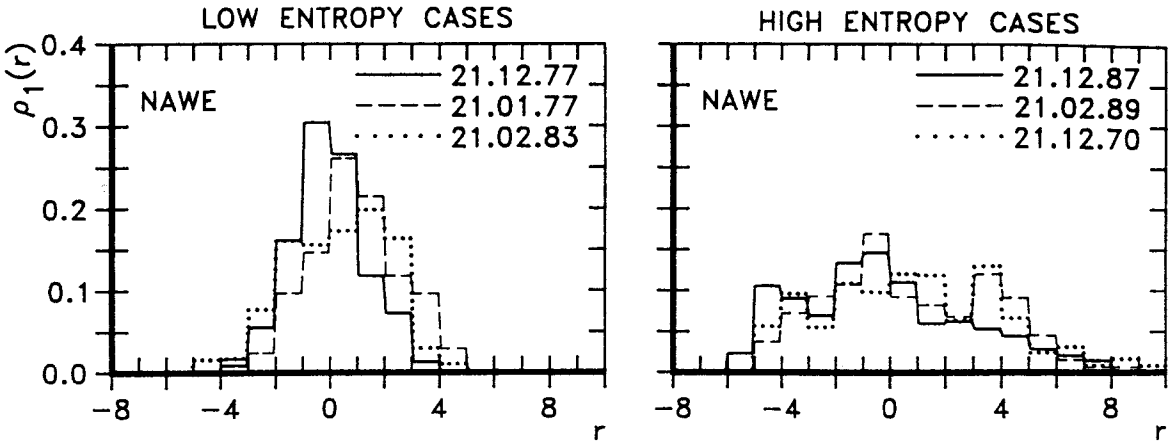
LOW ENTROPY CASES
HIGH ENTROPY CASES
NAWE
NAWE
21.12.77
21.01.77
21.02.83
21.12.87
21.02.89
21.12.70
$\rho_1(r)$
0.4
0.3
0.2
0.1
0.0
−8
−4
0
4
8
r

123SLKa

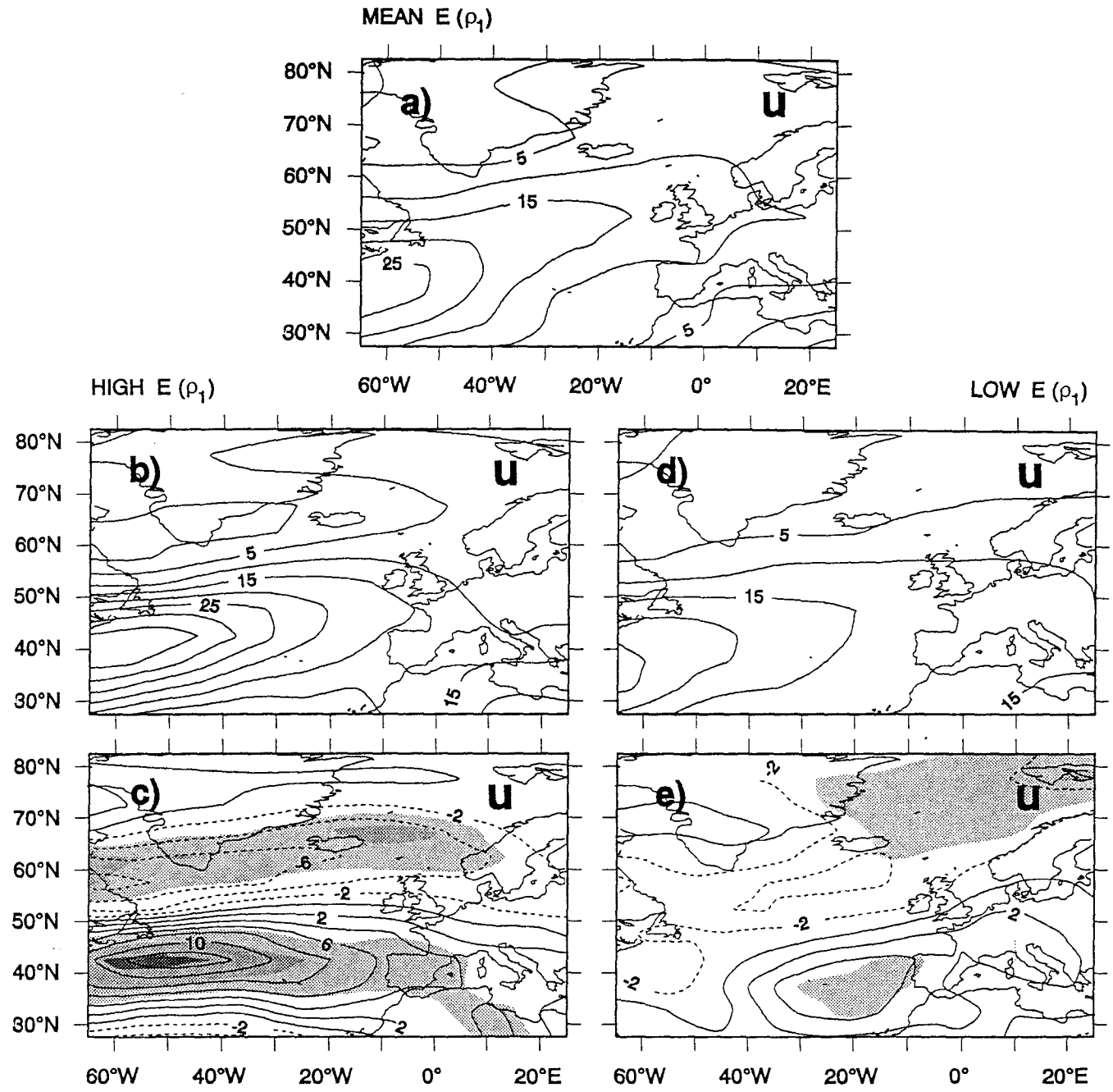

123SLKbb.drw

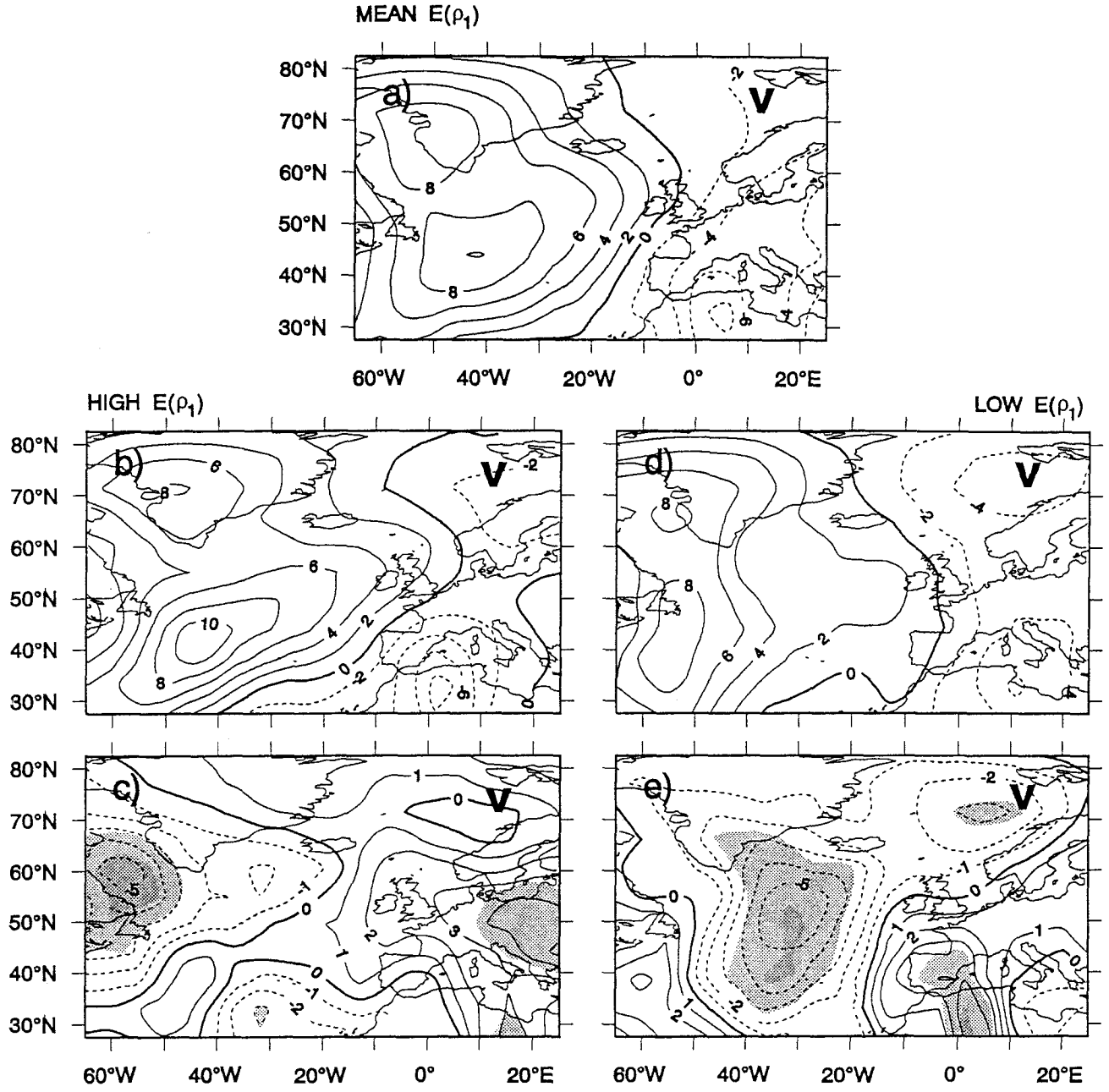

014SLKc.drw

(014SLKb)

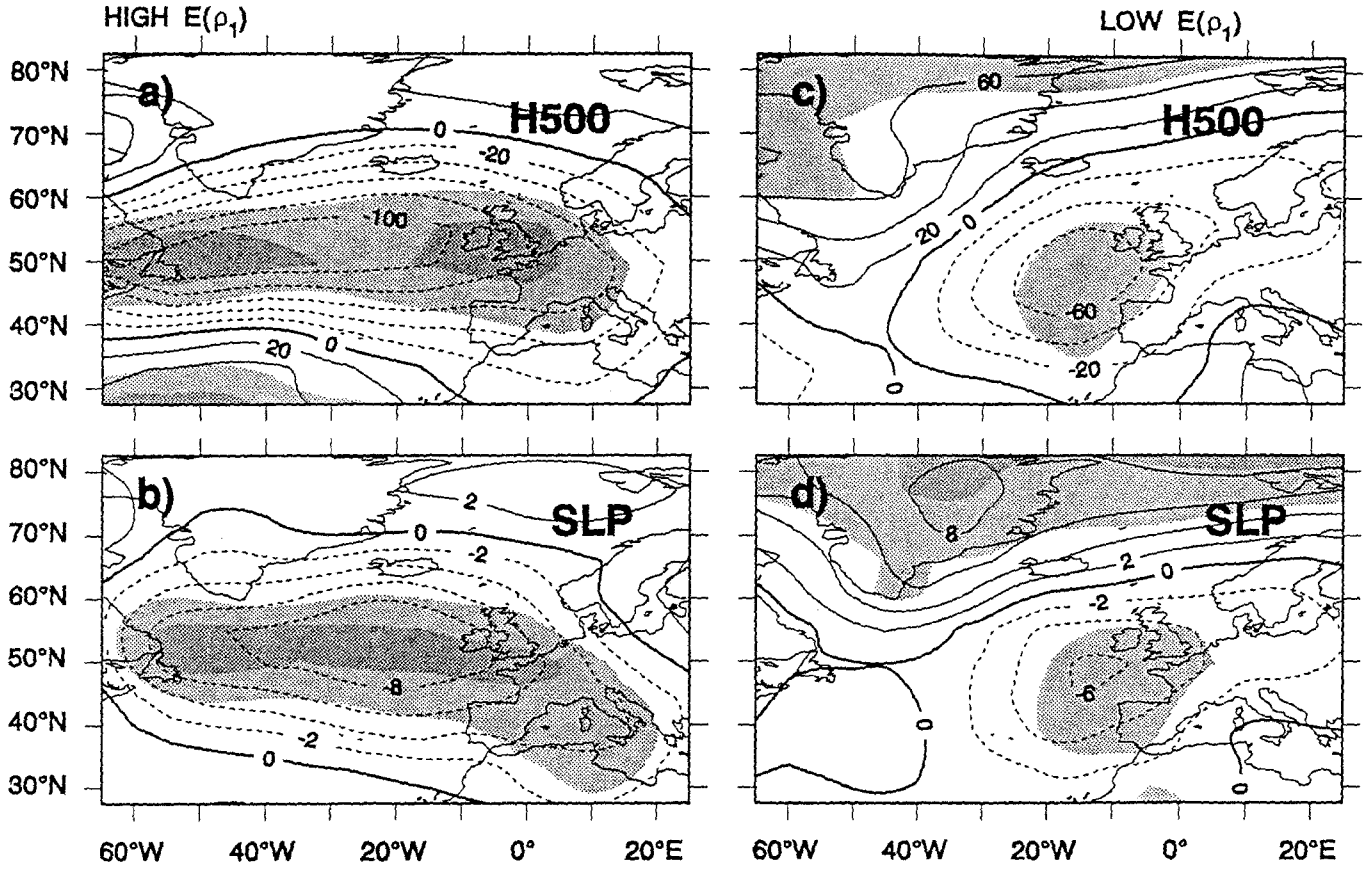

024SLKa.drw
(014SLKb)

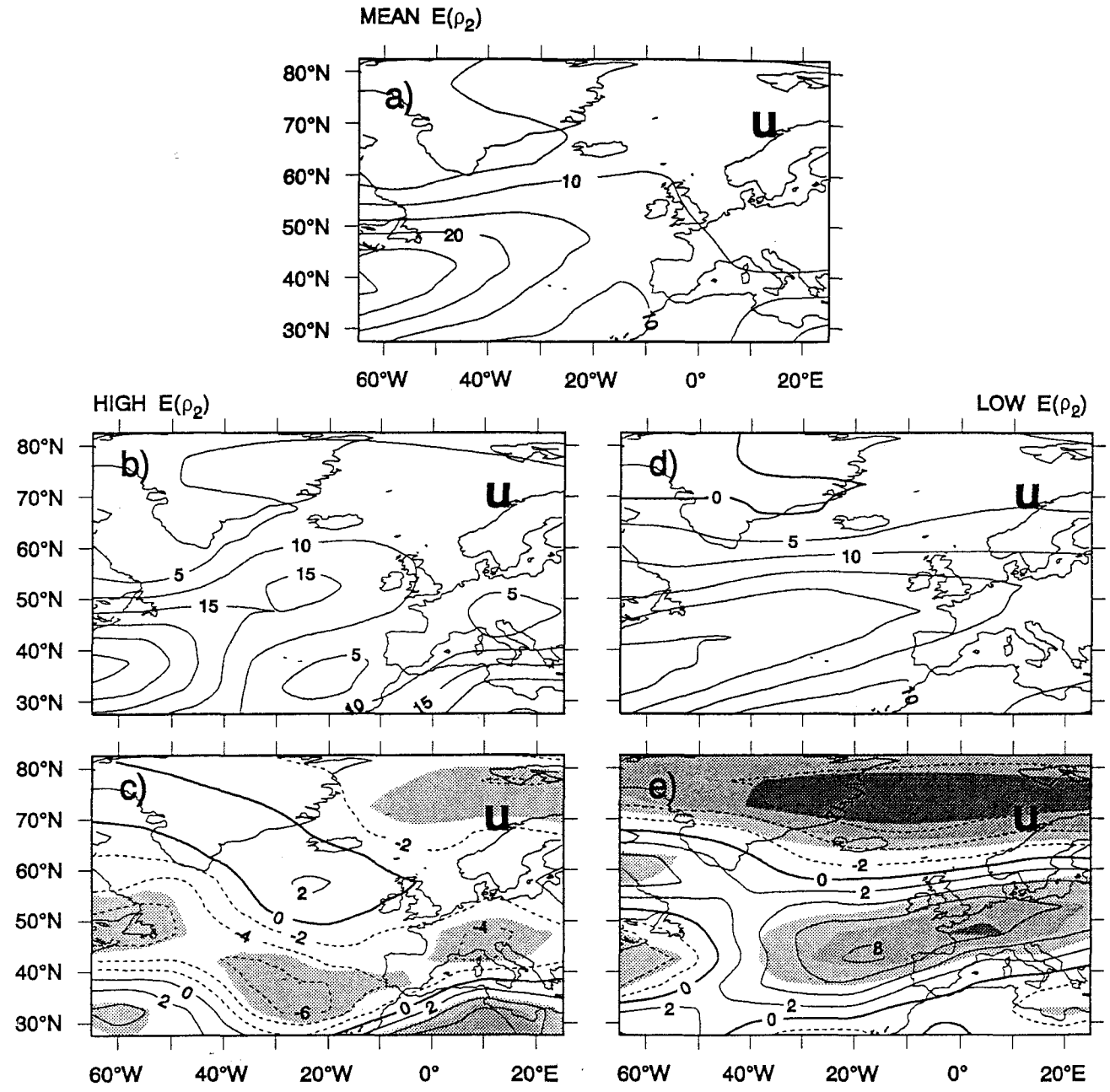

014SLKd.drw

(014SLKb)

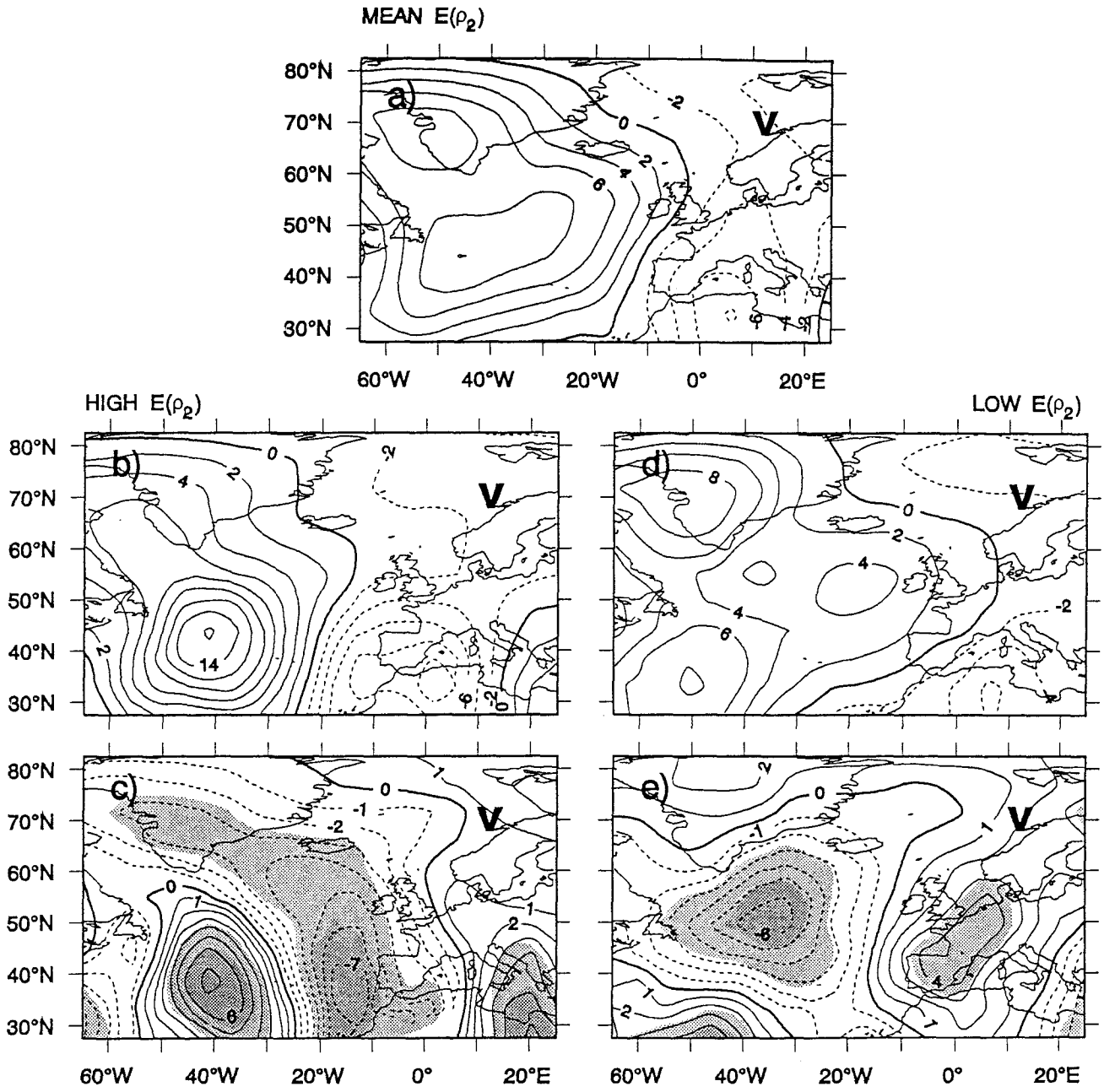

014SLKa.drw

(014SLKb)

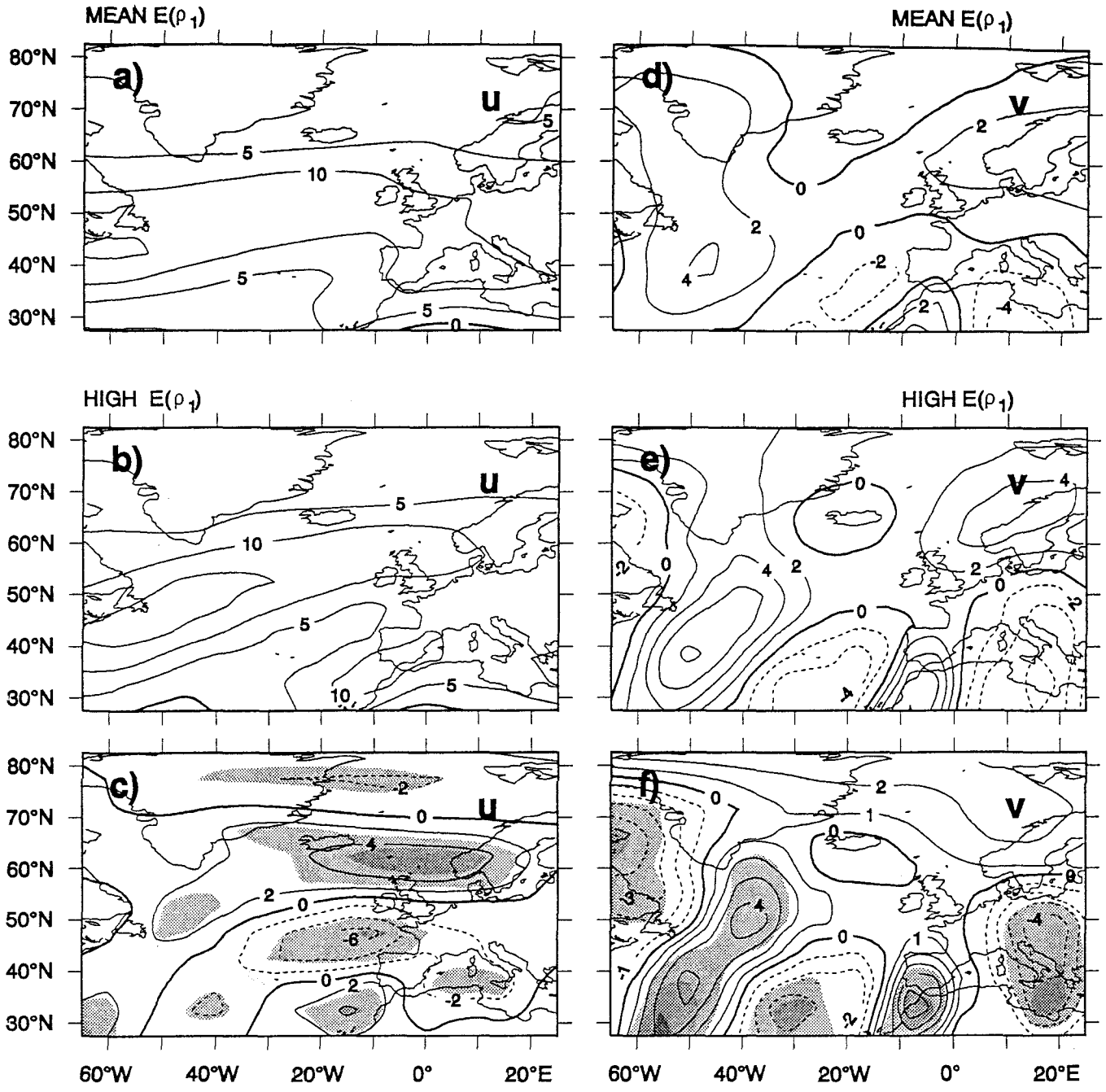

024SLKc.drw

(024SLKb)

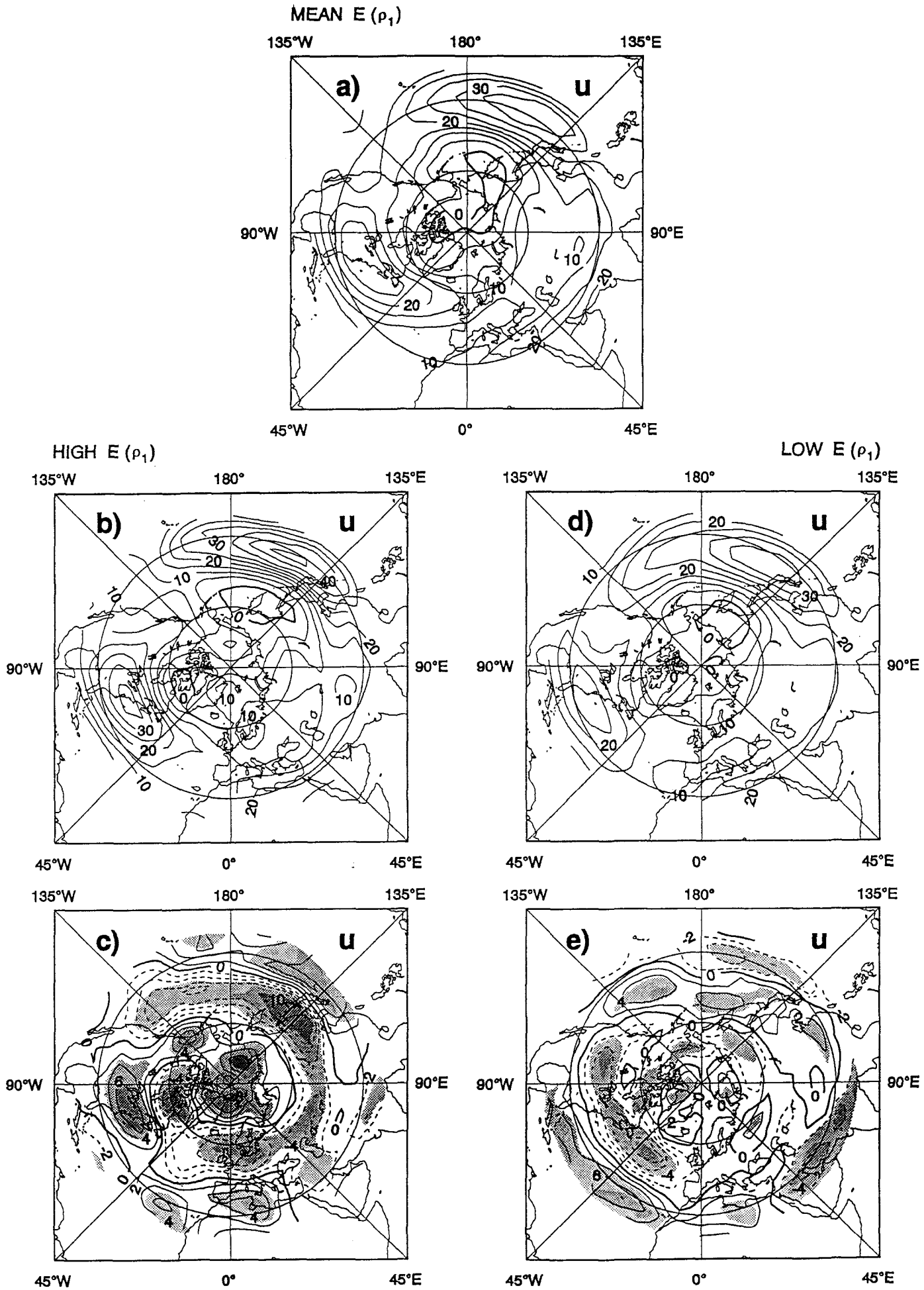

024SLKfa.drw

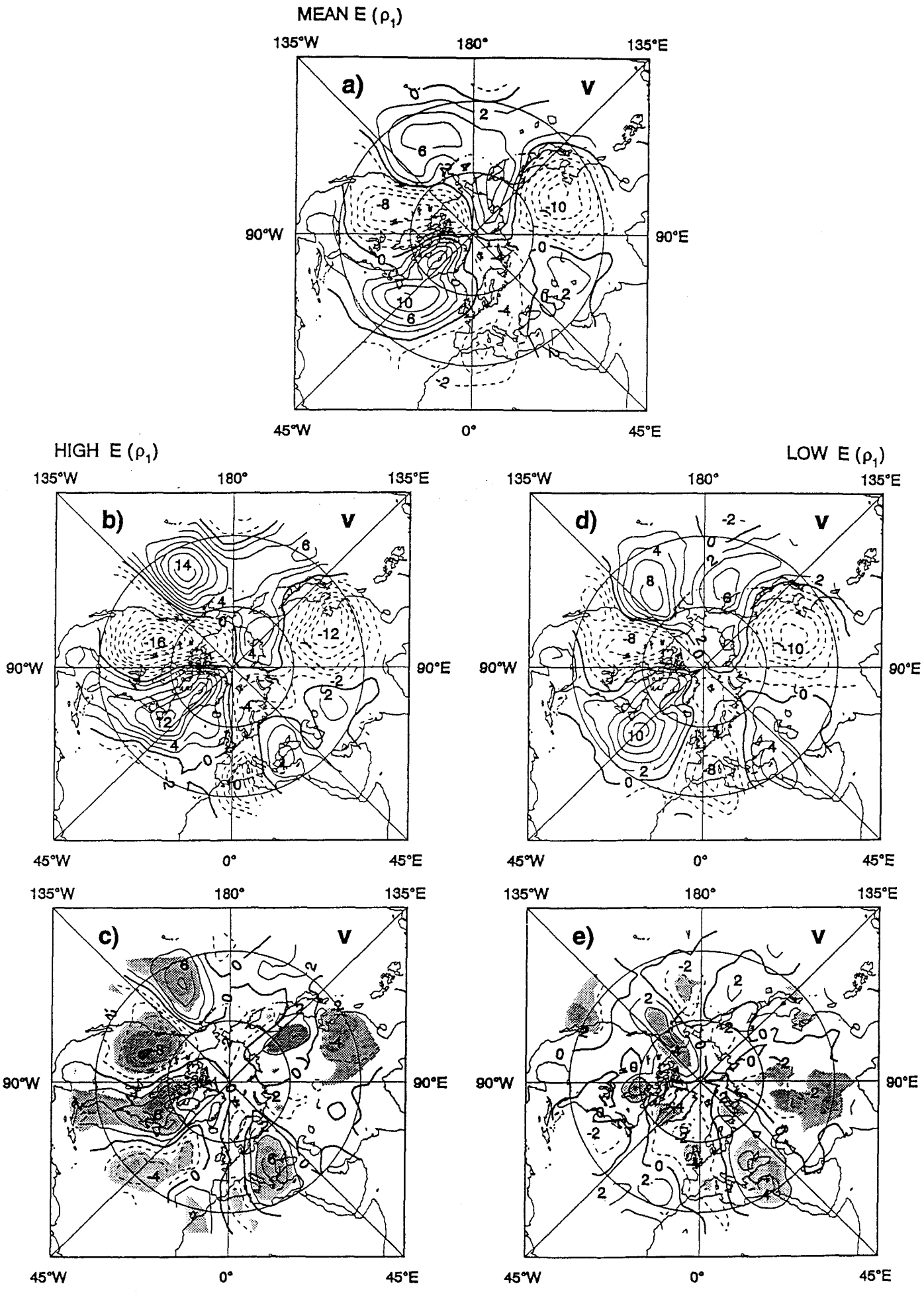
MEAN E (ρ_1)
135°W
180°
135°E
a)
v
90°W
90°E
45°W
0°
45°E
HIGH E (ρ_1)
b)
LOW E (ρ_1)
d)
c)
e)

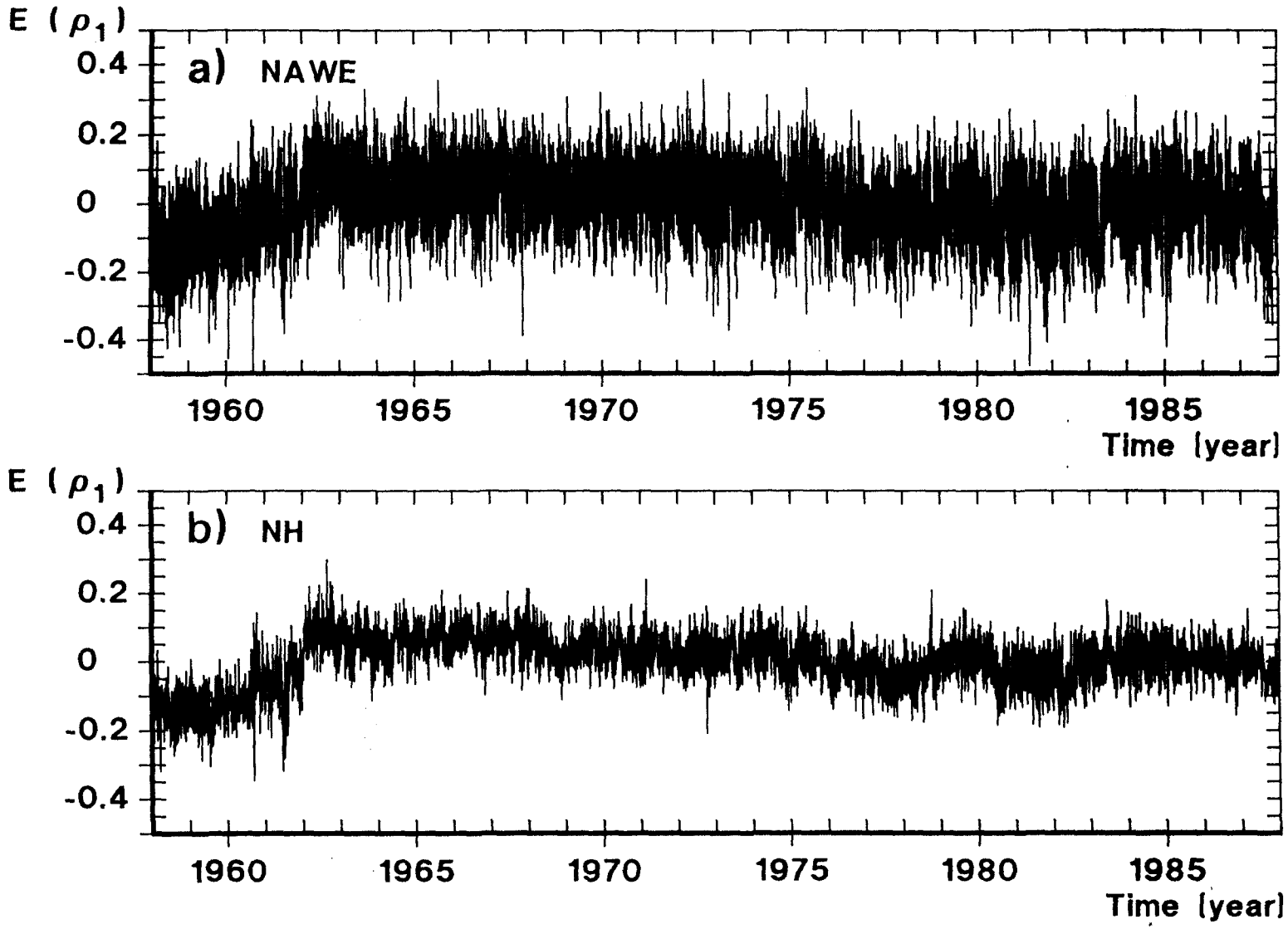

024SLKd

Fig 13

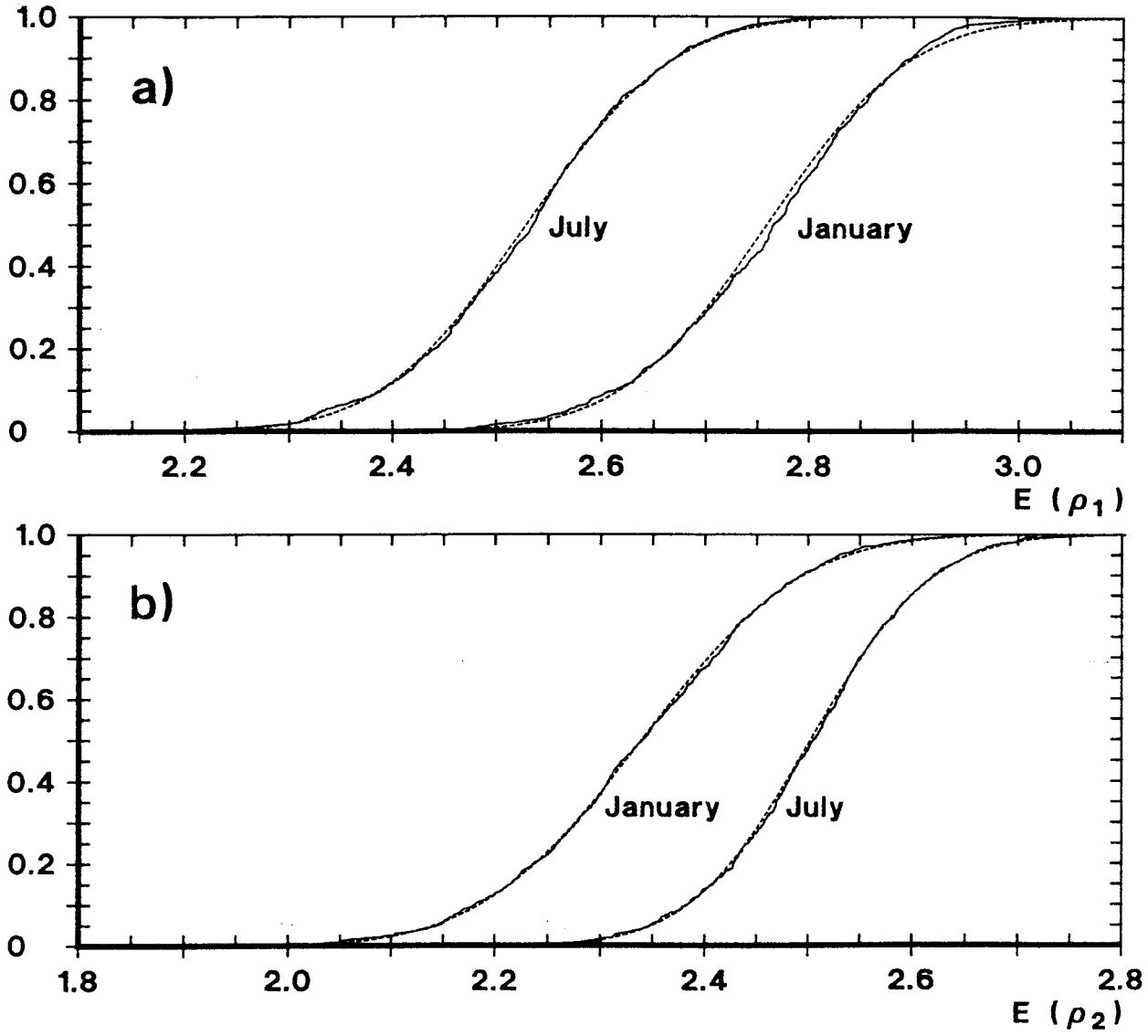
a)
1.0
0.8
0.6
0.4
0.2
0
July
January
2.2
2.4
2.6
2.8
3.0
E (ρ_1)
b)
1.0
0.8
0.6
0.4
0.2
0
January
July
1.8
2.0
2.2
2.4
2.6
2.8
E (ρ_2)

024SLKe